DEPOSITION OF IONIC LIQUID THIN FILMS ONTO SELF-ASSEMBLED MONOLAYERS

By

Angeline Cione

Thesis

Submitted to the Faculty of the

Graduate School of Vanderbilt University

in partial fulfillment of the requirements

for the degree of

MASTER OF SCIENCE

in

Chemical Engineering

May, 2007

Nashville, Tennessee

G. Kane Jennings

Clare McCabe

To the Jennings Group, past present and future.

ACKNOWLEDGEMENTS

First and foremost, I would like to acknowledge and thank Kane Jennings for being the ideal advisor in his ability to be encouraging and understanding while having high expectations. He allowed me the freedom necessary to intellectually challenge myself but provided enough guidance that I was able to accomplish this work in the short time allotted. He is someone I truly admire and respect, not only for his professional ambitions and excellence, but also for his genuine concern and compassion for those around him.

I would also like to acknowledge and thank Bridget Rogers, as I would not be here if it weren't for her encouragement and her faith in me. She introduced me to chemical engineering and helped me continue my studies in the field. She has always been a trusted advisor and friend.

I have enjoyed working with the chemical engineering department at Vanderbilt University over the past four years. Both my undergraduate class and my graduate class have been very supportive, and in them I found great colleagues and friends. Thanks to my group, Brad, Chris, and Dongshun, I enjoyed coming into lab everyday. Brad performed the NMR experiments presented in this thesis, and he has been a great teacher who always explains things well. Chris showed me ropes when I first joined the group and helped me overcome many of the hurdles of research. Dongshun has also helped me through many research stumbling blocks and continually inspires me to work hard. Besides their assistance in the lab, I am thankful for the wisdom and humor shared with Dongshun, soapbox Thursdays with Chris, and office soccer with Brad.

I would also like to thank Ben, Nirav, Jimmy, Mekha, and Bridget Rogers for trekking down to the lab and allowing me to use the ellipsometer in their lab. Likewise, I'm grateful to Dr. Cliffel and his group, especially Madalina Ciobanu, for allowing me to use their microscope and camera. Thanks to Ron Reisenberg for sharing his knowledge and allowing me to use his lab to perform spin-coating experiments. Thanks also to Oleg and the newest members of the nanotribology group for their work regarding this project.

I really appreciate the time and insights Clare McCabe contributed to this thesis, including her work with Kane to acquire the grant that made it possible. Finally, I acknowledge financial support from the Office of Naval Research under Grant Number N00014-06-1-0624.

TABLE OF CONTENTS

LIST OF TABLES

Table Page

LIST OF FIGURES

CHAPTER I

INTRODUCTION

Miniaturization is a prominent trend in today's technological advances as can be seen as laptop sizes decrease and cell phones acquire the capabilities of home computers. As devices shrink, they exhibit an increasing surface area to volume ratio.[1] Where volume, or bulk, forces typically dominate in traditional devices, surface forces that are negligible in traditional devices, begin to have a significant impact on device performance when devices push down toward the micrometer and nanometer regime. These surface forces often lead to adhesion and friction which interferes with device functioning. For example, capillary effects arise in closely spaced device features and can cause significant adhesion between asperities, leading to device failure, or even causing an asperity to break. Effective lubrication systems must protect device surfaces against adhesion, friction, and wear that are induced by these forces. Traditional lubricants are too viscous to penetrate tiny features of these devices or to allow devices to function properly so new approaches to lubrication must be developed. Nano and microelectromechanical systems (NEMS and MEMS) are a significant component of the emerging technology that faces this issue involving nanoscale lubrication.

NEMS and MEMS (referred to as 'MEMS' in the rest of this thesis) are essentially tiny motors, in that a chemical or electrical signal induces them to perform mechanical work. One common example is the accelerometer that releases an air bag at a critical deceleration. MEMS devices are commercially used in pressure sensors, inkjet printers,

and projector displays. In the near future, MEMS are expected to be employed in telecommunications, radio frequency (RF) systems, and in medical and biomedical devices.[1]

Most MEMS devices are made from a silicon substrate, in a process similar to microchip fabrication. During a final stage of processing called the wet etch, capillary forces often cause adhesion between the closely-spaced, hydrophilic device surfaces. This phenomenon, termed "release stiction", has been addressed in several ways. Supercritical drying with CO_2 is one innovative method that eliminates the effect of capillary forces during the wet stage of processing, but it doesn't address adhesion that occurs during device operation. Surface roughening is a method that eliminates release stiction *and* reduces in-use adhesion by adding tiny dimples on the surfaces to reduce the adhesion force by reducing the area of contact.[1] A strategy that eliminates release stiction and also reduces both adhesion and friction involves lowering the surface energy by applying a hydrophobic coating to device surfaces. Molecularly thin hydrophobic coatings have been created via both Langmuir-Blodgett (L-B) and self-assembly methods to eliminate adhesion. Because L-B films are limited to 2-D surfaces and are only physically bound, self-assembled monolayers (SAMs) have proven a more robust and versatile candidate for coating the complex geometries often encountered in MEMS applications.[2]

Alkylsilane self-assembled monolayers (SAMs) are molecularly thin films composed of alkane chains with a silane-based head group that can covalently bind to silanol groups on a silicon oxide surface, as shown in Figure 1. The thickness of the film, or monolayer, can be controlled by choosing molecules whose chain length corresponds to the desired film thickness. Properties of the monolayer, such as surface energy, can be controlled by altering functional groups on the molecules.

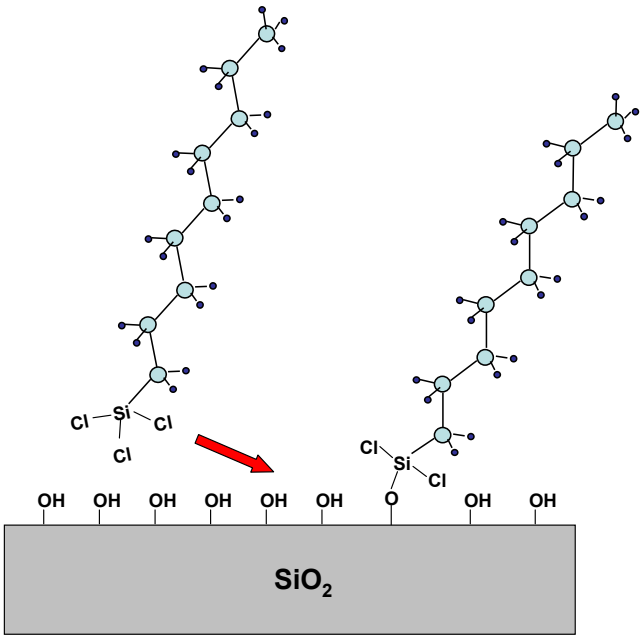

Figure 1a. *Alkyltrichlorosilane molecules covalently attach to a SiO_2 surface.*

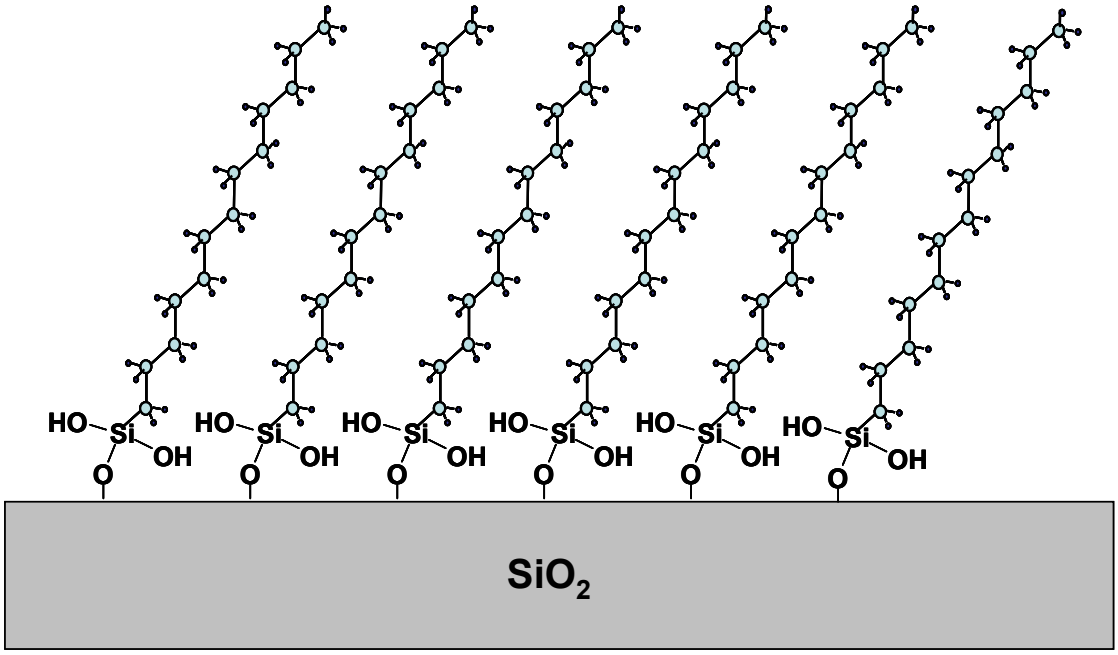

***Figure 1b**. A monolayer is formed via self-assembly of alkyltrichlorosilane molecules.*

Lubrication is necessary to prevent release stiction and also to reduce friction between components so they function properly. However, a lubrication scheme must also be robust so as to reduce the long-term wear on the device and extend its operational life. While hydrophobic SAMs have proven to eliminate adhesion and reduce friction, they wear away eventually and do not extend device life sufficiently. A mobile coating on top of a SAM could enhance lubrication by protecting the SAM layer and replenishing it as it is worn away.[2-8] The most commonly studied mobile layer is a PFPE (perfluoropolyether) coating, but another class of compounds, ionic liquids, may offer superior lubrication properties and greater versatility.[3]

Ionic liquids are ionic in nature like salts, but they are unique in that they are liquid at room temperature. Recently discovered, ionic liquids have a negligibly low vapor pressure, a wide electrochemical window, and are non-combustible.[9] By altering the structure of the cation or choosing different cation-anion combinations, an ionic

liquid with desirable properties for a specific application can be designed or chosen. The most commonly studied ionic liquids have an imidazolium-based cation, many of which have shown good lubrication properties[10, 11] or even out-performed traditional lubricants.[12-14]

The work in this thesis investigates thin films of both SAMs and ionic liquids for the application of MEMS lubrication. SAMs were prepared from alkyltrichlorosilanes and alkanethiols and the ionic liquid 1-butyl-3-methylimidazolium triflate, [bmim$^+$][triflate$^-$], was prepared as an initial test case. The complexities of applying a thin film of [bmim$^+$][triflate$^-$] to a low-surface energy SAM were investigated.

CHAPTER II

BACKGROUND

Intermolecular and Surface Forces

As device features become smaller, approaching the nanometer scale and molecular dimensions, their surface to volume ratio becomes very large and their working parts are placed closer together. Because of this close spacing, intermolecular and surface forces that are negligible in larger devices become the dominant forces acting on device features. Intermolecular forces are typically quantified by the relation

$$F \propto 1/r^n, \qquad n > 3 \tag{1}$$

where F is the force between two objects, r is the distance between the two objects, and n varies depending on the type of force. For example, n = 7 for two non-polar molecules and n = 4 for fixed dipole-dipole interactions.[15] As described by Equation 1, intermolecular forces are large at very small separation distances, but many of these forces quickly decay at larger distances. Therefore, these forces are typically negligible in traditional devices that have working parts separated by larger distances or have much stronger restoring forces due to larger feature size. However, when device features are separated by a distance of a few nanometers and approach molecular contact, intermolecular and surface forces have a significant impact on the functioning of the device. In many cases, this close spacing is the heart of nano scale devices; they are designed so that electrostatic forces induce their small features to do work. However,

other intermolecular forces can cause unwanted interactions, such as adhesion between features.

Intermolecular forces can be loosely classified as electrostatic, polar, induced polarization, and quantum mechanical in nature[15]. Electrostatic interactions take place between charged particles. Polar forces take place between dipoles, quadrupoles, etc., and thus they largely describe the interactions of polar molecules. Induced polarization forces arise from induced dipole moments and tend to be the dominant forces in non-polar molecules. Quantum mechanical forces lead to chemical bonding and steric repulsion.

When many molecules are combined, as in a bulk fluid or at a surface, solvation forces or surface forces, respectively, arise due to the sum of the intermolecular forces acting there. Thus, polar fluids and polar surfaces will be dominated by polar interactions, and non-polar fluids and surfaces will be dominated by polarization forces. As a general rule, polar phases interact strongly with other polar phases, while non-polar phases interact strongly with other non-polar phases.

The interactions that occur at the boundary between two phases, S and L, are most easily understood in terms of interfacial free energy, γ_{SL} (depicted in Figure 2) which describes the energy of the interface. Because systems tend towards the minimization of free energy, interfaces with the lowest energy will dominate. Thus, the most mobile phases in a system arrange themselves to maximize contact area at the interfaces with the lowest interfacial free energy.

For example, consider a system containing a solid surface, S, exposed to both a vapor phase V, and a liquid phase, L, as depicted in Figure 2. The system has three interfaces with interfacial energies of γ_{SV}, γ_{SL}, and γ_{LV}.

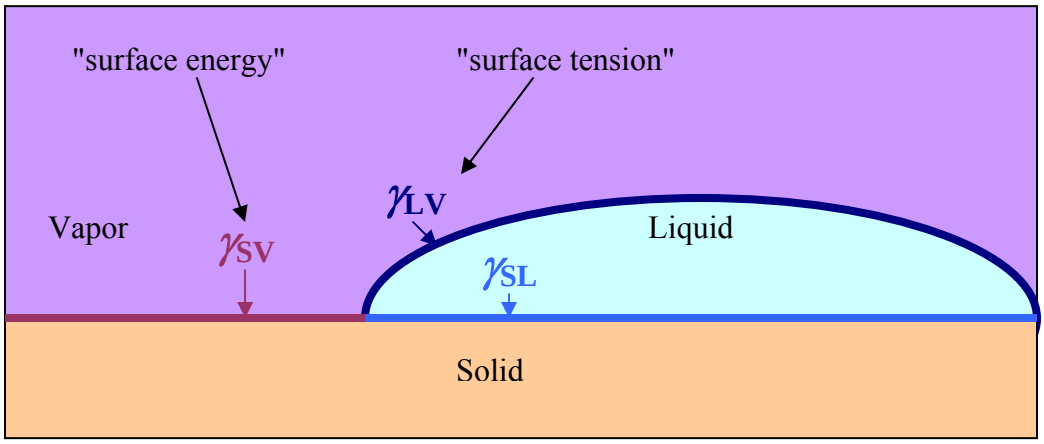

Figure 2. *Interfacial energies in a system describe the stability of a given interface.*

Generally, in air, γ_{SV} describes the surface energy of the solid, and γ_{LV} is the surface tension of a liquid. When a surface energy, γ_{SV}, is said to be low, the solid-vapor interface is in a low energy state and the surface is relatively stable. If liquid were placed on the surface, the low-energy solid-vapor interface would maximize its area causing the liquid to bead up on the surface. Conversely, a liquid spreads across a high-energy surface, expanding the contact area of lower-energy solid-liquid interface. This behavior is described by the spreading coefficient, S, in the equation,

$$S = \gamma_{SV} - (\gamma_{SL} + \gamma_{LV}) \geq 0, \qquad (2)$$

which is used to describe whether a liquid will spread across a surface. When $S \geq 0$, the liquid will spontaneously spread across the surface, but when $S < 0$ the liquid will not spread. Thus, increasing surface energy, γ_{SV}, and decreasing surface tension, γ_{LV}, promotes spreading.

The wetting properties described above can be quantified further by measuring the contact angle of a liquid on a surface. Dynamic contact angles are measured as a

liquid advances or recedes across a surface, as shown in Figure 3. The contact angle of a liquid relates to interfacial free energies, as stated by Young's equation,

$$\cos \theta = (\gamma_{SV} - \gamma_{SL}) / \gamma_{LV}, \quad (3)$$

where θ is the contact angle, and γ_{SV}, γ_{SL}, and γ_{LV} are defined as above. Young's equation states that for a given liquid, when the surface energy, γ_{SV}, is higher than γ_{SL}, the contact angle will be lower than 90°, and when the surface energy, γ_{SV}, is lower than γ_{SL}, the contact angle will be greater than 90°.

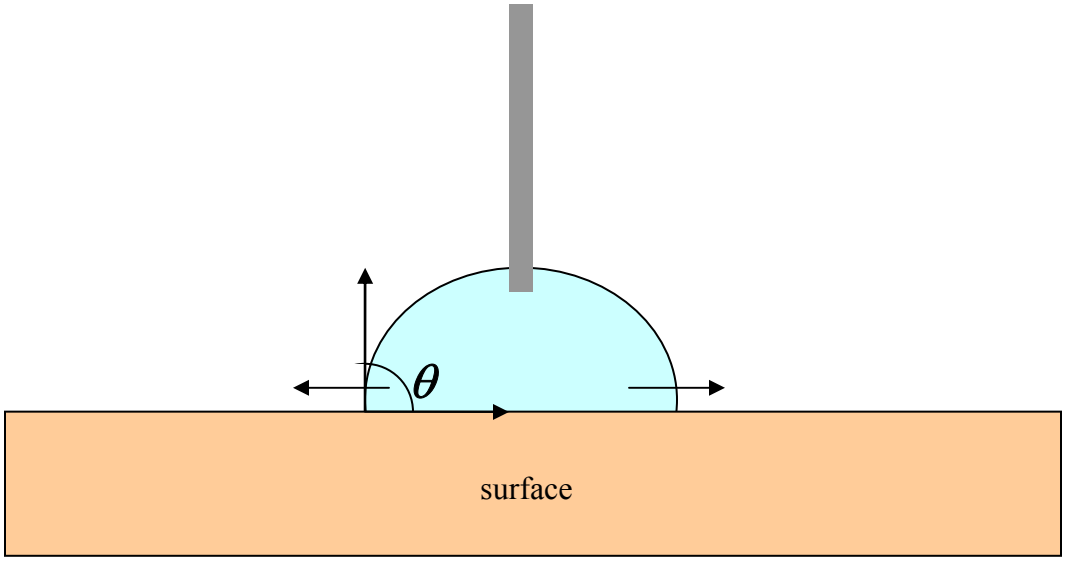

***Figure 3**. An advancing contact angle, θ, is measured as liquid advances across a surface while being expelled from a syringe needle. The receding contact angle is measured by pulling the liquid back into the syringe so that it moves in the opposite direction.*

Contact angle analysis is a very useful surface characterization technique because it can be used not only to estimate surface energy, but also to predict the strength of capillary forces and adhesion forces. The phenomenon of capillarity occurs when liquid

is confined between two closely spaced solids. The height a liquid rises in a capillary tube can be described by the LaPlace equation,

$$h = 2\ \gamma_{LV} \cos\theta\ /\ (\rho\ g\ r) \qquad (4)$$

where h is height of capillarity, γ_{LV} is the surface tension of the liquid, θ is the contact angle of the liquid on the solid, ρ is the density of the liquid, g is the gravitational force constant, and r is radius of the capillary tube. Generalizing the relationship to other geometries, high surface energy ($\theta < 90°$) and close spacing between surfaces (small r) increases capillarity while low surface energy ($\theta > 90°$) reverses capillarity.

Contact angle analysis can also be used to quantify adhesion forces between two surfaces. When two surfaces are in contact, the work of adhesion, W_a, is the work required to separate the two surfaces into two phases. The Dupre equation,

$$W_a = \gamma_A + \gamma_B - \gamma_{AB} = \gamma_L\ (1 + \cos\theta) \qquad (5)$$

(where γ_L is the surface tension of the liquid used to measure the contact angle and A and B are two surfaces) shows that high energy surfaces ($\theta < 90°$) undergo stronger adhesion than two low energy surfaces.

Stiction, Adhesion, Friction and Wear in MEMS

The four critical issues in MEMS that must be addressed by lubrication are stiction ("release stiction"), adhesion ("in-use stiction"), friction, and wear.

Stiction, or "release stiction," occurs when capillary forces cause closely-spaced features to adhere to each other. This adhesion often leads to device failure, as it can cause a feature to fracture or break off completely. Release stiction is often a problem during the final stages of device fabrication, when the presence of liquid, (generally from

a wet etch), gives rise to capillary forces. Besides processing without liquids (by using supercritical CO_2) or adding dimples to roughen the surface, the most common and effective means of eliminating stiction is to coat devices with a hydrophobic coating that reduces the work of adhesion between surfaces.[16]

Adhesion or "in-use stiction" is due to the adhesion that occurs between asperities or surfaces that are separated by small distances. Simulations show that the adhesive forces between closely spaced solid surfaces can cause them to "jump towards each other" and plastically deform in a similar way that interfacial forces between a liquid and solid cause the liquid to wet the solid surface.[17] These adhesive forces can be described by equation (3), above. The right hand side of equation 3,

$$W_a = \gamma_L (1 + \cos \theta) \qquad (3b)$$

clearly shows that coatings with low surface energy (θ>90°) have lower work of adhesion. Therefore, lowering the surface energy can minimize the adhesive forces between surfaces in the same way that it can eliminate release stiction.

Adhesion and friction in nanoscale devices is a sticky situation. For example, a liquid film between two surfaces can potentially either reduce or *cause* adhesion and friction. Due to the capillary effect, a thin liquid film between two surfaces can cause adhesion, as in release stiction. However, a thin liquid film may also maintain a lubricating layer between surfaces to prevent adhesion, as in traditional lubrication. Similarly, during nanoscale sliding, a liquid layer may act as a lubricating layer and reduce friction, or it may solidify upon sliding and lead to increased friction.

Understanding the mechanisms of friction and lubrication at the nanometer and micron scales has proven to be a complex task because the classical geometric laws of

friction (Amonton's laws) do not suffice in describing friction on the nanometer scale. Amonton's laws state that the friction coefficient is independent of contact area, load, and sliding velocity. However, on the nanometer scale, minimizing load and area of contact minimizes friction. For example, as mentioned previously, adhesion and friction have been reduced by creating slight surface imperfections (or roughness) to reduce the real area of contact.[16]

The reason for the discontinuity between macroscale and microscale friction models was alluded to previously. On the macroscale, intermolecular forces are negligible because externally applied forces are orders of magnitude higher, rendering intermolecular forces insignificant. However, when the externally applied force is on the same order of magnitude as the intermolecular and surface forces inherent to the system, those forces play a significant role in the system response. In the case of friction, intermolecular and surface forces describe the mechanisms of energy dissipation that cause friction on the nanoscale. Because Amonton's laws are geometrically based and do not account for energy dissipation, the classical friction model does not suffice in describing and predicting nanoscale friction. Instead, nanoscale friction must be described by new models that incorporate molecular mechanisms of energy transfer.

Solid coatings have been shown to reduce friction,[18, 19] but systems with high mobility have also reduced friction and increased wear life.[2, 3, 6, 8] Yoshizawa et al. explained this phenomenon by defining friction states in surface films as a continuum with the three different regions of liquidity, amorphous crystallinity, and solid crystallinity.[20] Of these three regions, the two extremes, liquidity and solid crystallinity, are states of low friction, whereas the amorphous crystalline region is characterized by

high friction, as shown in Figure 4. More specifically, films in the liquid region are composed of mobile molecules with very fast relaxation times. Upon sliding, the molecules flow (Coutte flow) allowing the surfaces to smoothly slide past each other. Thus, films in the liquid region experience a constant low sliding friction that increases slightly with increasing sliding velocity. Films in the amorphous crystalline region experience high, erratic frictional behavior due to interdigitation of the molecules and long relaxation times relative to the sliding velocity. Films in the solid region have low friction as the two smooth surfaces slide past each other, but they are also characterized by oscillatory friction. This "stick-slip" behavior occurs as the molecules between the two sliding surfaces alternately “freeze up” and liquefy upon sliding. The solid films have a high relaxation time so the oscillatory behavior increases in frequency then fades into constant low friction as sliding velocity increases.

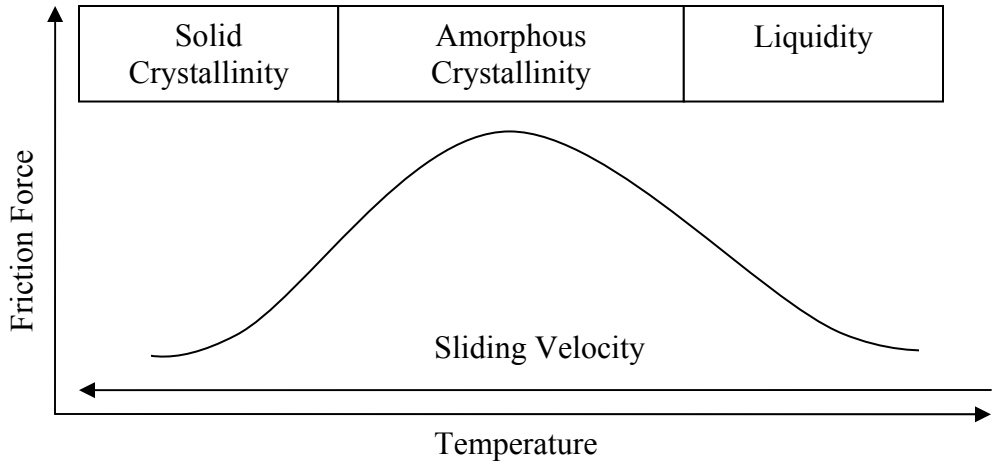

Figure 4. *Model of friction on the nanoscale, as proposed by Yoshizawa. When load and area of contact are held constant frictional behavior on the nanometer scale is dependent on sliding velocity and temperature as shown above. Surfaces transition between molecular conformational states of solid crystallinity, amorphous crystallinity, and liquidity upon changes in sliding velocity and temperature as shown above.*

As stated previously, a liquid film between two surfaces can either increase or reduce friction. The model described above addresses this ambiguous behavior by correlating friction to the phase state of the film. When a thin film is confined between two surfaces its state is dependent on the relative velocity of the two surfaces and film temperature (assuming constant load and area of contact).[17] A confined film in the liquid state will transition to a high-friction, amorphous crystalline state at high sliding velocities and/or low temperatures. Similarly, a high-friction amorphous film may transition to a low friction state if it can be driven into the solid or liquid regime by changing the sliding velocity and/or temperature. Thus unlike macroscale surfaces that have a constant frictional coefficient, the frictional coefficient of microscale surfaces will vary with sliding velocity, temperature, area of contact, and applied load. Therefore,

rather than one universal method for lubricating MEMS devices, different lubrication schemes may be tailored to specific applications, based on force and frequency of contact, size of contacting asperities, sliding velocity, operating conditions (temperature, humidity, chemical environment), and manufacturing capabilities.

While high friction and adhesion leads to increased wear and device failure, durability of the surface is also an important factor affecting wear. Wear refers to damage to a device caused by applied stresses during normal operation, and wear life refers to the lifetime of a device that fails due to wear. Friction and adhesion are generally the causes of wear, but many experimental results demonstrate that the lowest friction film is not necessarily the most wear-resistant.[2, 3, 8] Therefore, lubrication schemes, in general, should reduce adhesion and friction but also be long-lasting, robust coatings that resist wear.

Ionic Liquids

Most ionic compounds are solid at room temperature because they pack into crystalline structures that drive up their melting temperature. Recently discovered, room temperature ionic liquids (ILs) are unique ionic compounds that have a bulky, asymmetric organic cation (or anion) that inhibits crystalline packing, leading to low melting temperatures. ILs are uniquely flexible in that the properties of the liquid can be tuned by choosing a different cation or anion. Other significant properties of ILs include a negligibly low vapor pressure, non-combustibility, and a wide electrochemical window[9]. Because of these properties, ILs have found many applications including

nonvolatile solvents, electrolytes, and lubricants. In many cases, especially in lubrication studies,[10, 12, 21] ILs have outperformed traditional chemicals.[9, 22]

Imidazolium-based ILs are the most commonly studied system because of their air and moisture stability.[9, 23] The ionic liquids with the 1-n-alkyl-3-methylimidazolium cation and either the BF_4 or PF_6 anion have proven to be effective lubricants in many studies.[10-12, 24, 25] Figure 5 depicts the structure of these molecules and lists some common anions and common terminology. It has been suggested that fluorinated anions may decompose to form fluorides that protect surfaces from further wear.[12] Jimenez showed that the triflate anion, CF_3SO_3, has better wear-reducing properties than BF_4 or PF_6.[11] He also showed that cations with longer side chains (n > 2) improved wear properties even more than changing the anion.

Common side chains, R_1	Cation Abbr, when $R_3=CH_3$
methyl	mmim
ethyl	emim
butyl	bmim
hexyl	hmim
octyl	omim

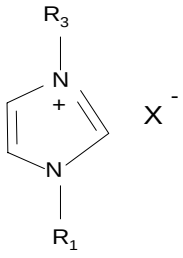

1-R_1-3-R_3imidazolium X

Common Anions, X
PF_6^-
BF_4^-
NO_3^-
$[CF_3SO_3]^-$
$[N(CF_3SO_2)_2]^-$

Figure 5*. Structure and nomenclature of common imidazolium ionic liquids*

Because they have demonstrated good lubrication properties, ionic liquids may be an effective lubricant in MEMS devices as well. In previous studies, perfluoropolyethers

(PFPEs) have effectively been used as mobile films for MEMS lubrication. However, ILs may be a superior lubricant because they have lower volatility, good low-temperature fluidity, and good lubricity in air or in vacuum.[12] In some MEMS devices, such as RF switches, charge build-up reduces device reliability,[26] and the conductive nature of an IL coating may eliminate this problem.

Self-Assembled Monolayers

When molecules pack tightly into self assembled monolayers (SAMs) of high conformational order, they form solid films that reduce friction.[18] However, loosely-packed monolayers are in a more fluid state that is bound to the surface and exhibit higher friction which is characteristic of the amorphous crystalline region described by Yoshizawa.[20] Densely packed monolayers can be constructed on gold provided the substrate is in solution long enough for the molecules to bind to the surface, orient into close-packed structures, and fill defect sites. Trichlorosilane SAMs have the same requirements, but they must also be formed in the absence of water on hydroxylated Si surfaces. The presence of water in solution can cause polymerization of the molecules, inhibiting close-packed monolayer formation as depicted in Figure 6. Poorly packed monolayers lead to rough surfaces that do not provide a good film barrier to the substrate, are more prone to chemical attack, and wear away easily. However, densely packed monolayers exhibit the opposite properties and resemble solid films.

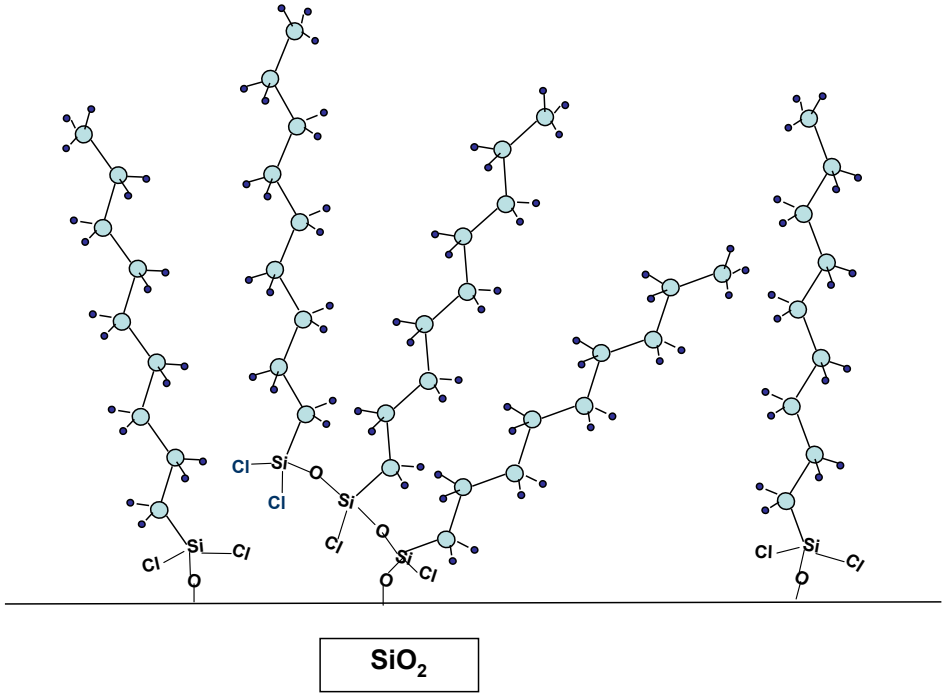

Figure 6*. Polymerization of trichlorosilane molecules creates defects, prevening the formation of smooth, tightly-packed monolayers.*

Lubrication Schemes for MEMS

While many studies have shown that liquid coatings of perfluoropolyethers (PFPEs) have reduced friction and wear in MEMS devices,[2, 5-8] they don't significantly increase the critical load or scratch resistance of a surface because they lack hardness.[5] On the other hand, SAMs have higher hardness than mobile layers and increase the critical load while reducing friction and wear because they are in the solid crystalline state described by Yoshizawa et al.[20] However, SAMs have not *sufficiently* extended the operational life of MEMS because they are worn away after some time. An ideal lubrication scheme would incorporate a bound SAM coating of low surface energy and

high hardness, with a friction-reducing, mobile layer to fill in defects and replenish the bound layer as it is worn away.

However, surfaces with low surface energy resist wetting so mobile films may not coat hydrophobic SAMs. For a mobile coating to effectively coat and replenish an underlying film, the two coatings must be compatible.[7] The importance of good interactions between the bound and mobile films was demonstrated by Satyanarayana et al[2] . They found that a thin mobile film of Fomblin Zdol on a hydrophobic SAM did not enhance the SAMs lubrication ability, but the mobile layer on a *hydrophilic* SAM reduced friction significantly. While use of a hydrophilic SAM may not be practical because it will cause stiction and adhesion problems, a SAM that is too hydrophobic will not allow for a mobile, replenishing layer to aid lubrication. A mobile layer that has favorable interfacial interactions with a solid SAM surface is needed. This issue is explored in the following work.

CHAPTER III

METHODS

Materials

All water was deionized (DI), purified to 16.7 MOhms·cm with a Modu-Pure system. Samples were dried with compressed N_2. Anhydrous dichloromethane and anhydrous toluene were purchased from Fisher. Anhydrous chloroform (99%), methyl trifluoromethane sulfonate (98%), butyl imidazole (98%) anhydrous THF, borane-THF complex, ammonium hydroxide, 1-octadecanethiol, 1-dodecanethiol, 1-octanethiol, 11-mercapto-1-undecanol, and 11-mercapto-1-undecanoic acid were purchased from Aldrich. (Tridecafluoro-1,1,2,2-tetrahydrooctyl)-1-trichlorosilane, octyltrichlorosilane, and octadecyltrichlorosilane were purchased from United Chemical Technologies (UCT), and 5-hexenyltrichlorosilane, 7-octenyltrichlorosilane, dodecyltrichlorosilane, and hexadecyltrichlorosilane were purchased from Gelest. Silicon wafers (100) were purchased from Montco Silicon. NaCl crystals and cover slips (used to do transmission IR spectroscopy on the ionic liquid) were from International Crystal Labs.

Procedures

[bmim$^+$][triflate$^-$] (IL) Preparation

In this investigation, the ionic liquid, 1-butyl-4-methylimidazolium trifluoromethanesulfonate ([bmim$^+$][triflate$^-$]) was used. The structure of this molecule is depicted in Figure 7. The procedure for the synthesis of the ionic liquid, [bmim][triflate],

(referred to as the IL in the rest of the document), was adapted from a procedure reported by Bonhote[27].

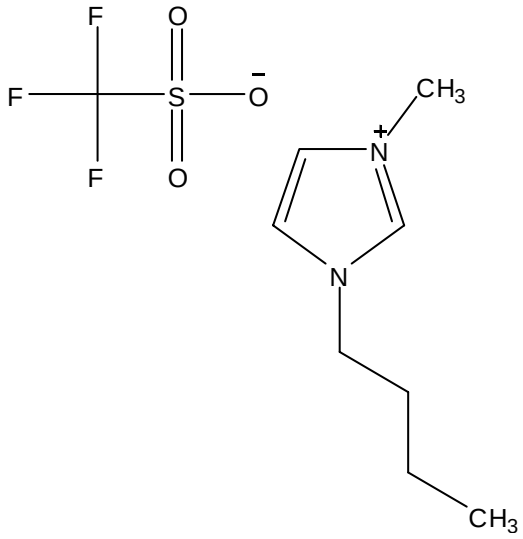

Figure 7. *Structure of bmim triflate*

Under nitrogen atmosphere, ~120mL of anhydrous dichloromethane was added to 50g of methyl triflate (for ~2.5M solution). This methyl triflate solution was added, dropwise, to 42 mL (~0.3 mol, or 38g) of 1-butylimidazole under a nitrogen atmosphere and stirred vigorously in an ice bath. Dichloromethane and water were evaporated from the resulting single phase liquid using a Rotavap for ~1 h followed by placement on the vacuum line overnight. The final product was stored under nitrogen atmosphere and characterized using NMR analysis. ^{1}H NMR (400 MHz, $CDCl_3$): δ 0.916 (3H), 1.30 (2H), 1.83 (2H), 3.93 (3H), 4.16 (2H), 7.38 (2H), 9.03 (1H). These results are consistent with those reported by Bonhote.[27]

Silicon Sample Preparation

Sample substrates were prepared from Si wafers cut into ~4 cm x 1.3 cm pieces. The samples were sonicated in soapy water for 30 minutes, rinsed with water, dried, and placed in piranha solution (14mL H_2SO_4:6mL H_2O_2) for 30 min to 1 h to remove adventitious carbon and hydroxylate the SiO_2 into silanols that react with trichlorosilane head groups. Samples were rinsed 3 times by submersion in water. The first rinse was a 15 second submersion/agitation, followed immediately by submersion in a second rinse for 10 minutes, and a final submersion that lasted ~10-30 min until ellipsometry was performed on the sample and/or it was placed in precursor solution. Spectroscopic ellipsometry was performed on one sample from each Si wafer and/or from each set of experiments to determine the thickness of the oxide layer after piranha treatment. All samples were rinsed once more with DI water and thoroughly dried with N_2 before submersion in the precursor solution.

Precursor Solutions

For monolayer formation on silicon surfaces, 1mM solutions of silane precursor in anhydrous toluene or chloroform were prepared. These solvents were chosen because solvents with few or no methylene groups do not interfere with the packing of the alkane chains, allowing close-packed, well-ordered monolayers to be formed.[28] Much care was taken to keep water out of these solutions, and samples were thoroughly dried before submersion because water in these systems promotes polymerization of silanes, preventing well-packed monolayers from being formed.[29] While it has been found that a

small amount of water on the surface leads to higher film density,[30-32] the increased density is likely due to vertical polymerization rather than a more closely packed monolayer.[29, 33, 34]

To deposit self-assembled monolayers onto gold, gold substrates were exposed to 1mM solutions of an alkanethiol in ethanol for ~24 h. These solutions are not sensitive to water content and could be used for multiple weeks. For mixed monolayers, precursor solutions of dodecanethiol ($C_{12}SH$) with varying proportions of 11-mercapto-1undecanol ($HOC_{11}SH$) were prepared such that each mixture had a total thiol concentration of 1mM. Initially, mixtures of 0, 20%, 40%, 60%, 80%, and 100% (molar) $HOC_{11}SH$ were prepared from stock solutions of $C_{12}SH$ and $HOC_{11}SH$. To hone in on the critical composition that yielded a surface that would accept an ionic liquid film, mixtures of 80%, 85%, 90%, 95%, and 100% (molar) $HOC_{11}SH$ were prepared from new stock solutions. Finally, mixtures of 91%, 92%, 93%, and 94% (molar) $HOC_{11}SH$ were prepared from the latter stock solution. Two gold samples were placed in each solution for ~24 hours. Drop casting or contact angle analysis was performed immediately upon removing samples from solution and rinsing with water and drying in a stream of nitrogen.

The advancing water contact angle of each sample was measured to determine the fractional surface coverage of the monolayer from the equation proposed by Cassie,[35]

$$\cos \theta_{mixed} = \sigma_1 * \cos(\theta_1) + (1-\sigma_1) * \cos(\theta_2),$$

where θ_{mixed} is the water contact angle on the mixed monolayer, σ_i is the fractional coverage of species i in the monolayer, and θ_i is the water contact angle on a surface with 100% species i.

Drop Casting

A solution of 0.5%(w/v) ionic liquid in ethanol was prepared for drop casting. A plastic weigh boat was placed, upside down, in a 25 mL Erlenmeyer flask to provide a flat platform for the samples. Samples were placed on the platform, and a 10 μL drop was dropped in the center of the sample. The flask was immediately capped with a septum, secured with wire, and a needle was inserted into the septum to pull a vacuum on the flask. The flask was left under vacuum until the solvent was fully evaporated.

Characterization Techniques

Contact Angle Analysis

Water contact angles were used to quantify the hydrophobicity of a surface, and hexadecane contact angles were used to quantify the oleophobicity of a surface. Because of the polar nature of water, water contact angles are sensitive to the polarity on the surface. Likewise, due to the non-polar nature of hexadecane, hexadecane contact angles are sensitive to the polarizability of the surface.[36] For a surface coated with a monolayer of alkyl chains, contact angle analysis can probe the quality of near-surface chain-packing in the monolayer. The hexadecane contact angle will be high when a surface is fully covered with methyl groups, but hexadecane will wet a surface covered in non-polar methylene groups. A well-packed, oriented monolayer from a methyl-terminated adsorbate will predominately present methyl groups on the surface, so the hexadecane contact angle will be high. As a monolayer becomes less densely packed, methyl groups will expose the underlying methylene groups, and a decrease in the hexadecane contact

angle will be observed. Thus, contact angle analysis is useful in assessing the quality of a methyl-terminated monolayer on a surface.

In this study, the advancing and receding dynamic contact angles were measured with a Rame-Hart goniometer using a microliter syringe to apply DI water, hexadecane, or [bmim][triflate] (IL) as the probe fluid. The needle of the syringe remained inside the probe fluid droplet as the advancing and receding contact angle measurements were taken.

Spectroscopic Ellipsometry (SE)

Film thicknesses were measured using a J.A. Woollam XLS-100 variable angle spectroscopic ellipsometer. For each sample, 200 revs/meas were taken across a wavelength range of 400-600nm, at a 75° angle of incidence. WVASE 32 Version 3.374 software was used to model and calculate the thickness of the oxide layer and films.

For monolayers grown from a silicon surface, the sample surface was modeled as a 0.5mm Si substrate (using the software's pre-calculated "si" file,) with an oxide layer (modeled using the software's "SiO_2" file), and a Cauchy layer. The thickness of the oxide layer was approximated with a "point-by-point" fit on a piranha-treated sample. Films' thicknesses were calculated by modeling the sample with a Cauchy layer on top of the substrate and oxide layers described above. The thickness were fit to the data (with a "point-by-point" fit) approximating the index of refraction as 1.46. (The second Cauchy coefficient, B, was set to zero.) For samples that had a second film applied to them, the thickness of the first film was calculated and saved before a second, decoupled Cauchy layer was applied to the model and fit to the data using the same procedure.

For monolayers grown from gold, a fresh sample of gold was scanned, and a Cauchy fit of the n and k values were used to model the substrate. The monolayer thickness was approximated using the Cauchy model with the coefficients set at A=1.46, and B = C = 0. The thickness of the thin film coatings of IL were approximated using the Cauchy model with coefficients set to A = 1.434, and B = C = 0.

Infrared Spectroscopy (IR)

Infrared spectroscopy is a characterization technique in which a beam of infrared light is directed at a sample, and the wavelengths of the reflected or transmitted light give information about the chemical bonds present in the sample. Molecular bonds vibrate at frequencies that are within the range of frequencies characteristic of the infrared spectrum. The frequency of bond vibration varies depending on the nature of the atoms bonded together. Light that is of the same frequency as a bond's vibration may be absorbed by a molecule to induce stretching or wagging in the molecular bond. Because light is electromagnetic in nature, the incident IR light induces an electromagnetic field, and only molecular bonds with dipoles in the direction of the electric field are able to absorb energy.

Thin films can be characterized with reflectance-absorption infrared spectroscopy (RAIRS). In this method, incident light is directed onto the sample at an angle that produces an electromagnetic field normal to the surface. RAIRS is very sensitive to molecular orientation on surfaces because only transition dipole moments with a component directed perpendicular to the surface will contribute to the sample spectrum.

The instrument used is a Bio-Rad Excalibur FTS-3000 infrared spectrometer, with p-polarized light incident at 80° from the surface normal. Reflected light was detected with a nitrogen-cooled narrow-band MCT detector. A background spectrum was taken from a sample of deuterated octadecanethiol on gold. A second spectrum of the background sample was taken after it had been exposed to ambient air for a few seconds, and this was subtracted from each sample's spectrum to eliminate peaks due to ambient humidity. A spectrum of the bulk IL was acquired by replacing the RAIRS attachment in the spectrometer with a transmission attachment. A background spectrum was obtained using a clean NaCl crystal. A water spectrum was obtained by exposing the NaCl crystal to the ambient for a few seconds before obtaining another spectrum. A drop of IL was then placed on a NaCl crystal, and a transmission spectrum was immediately obtained using about 10 scans. The water spectrum was subtracted from the IL spectrum to account for ambient humidity.

Microscope Images

Microscope images of the ionic liquid thin films were acquired using an Olympus BX41 microscope with Pixera camera and Pixera Viewfinder Pro software.

CHAPTER IV

RESULTS AND DISCUSSION

Step 1: Monolayer Deposition on Gold and Silicon

SAMs on Gold

Most MEMS devices are currently fabricated from silicon, but many incorporate gold into their functions. For example, radio frequency (RF) switches in MEMS devices often consist of gold contacts. While gold has excellent properties for the switching function, the gold contacts experience high adhesion.[37] Hydrophobic self-assembled monolayers (SAMs) may be effective at eliminating these adhesional problems by reducing the surface energy. SAMs of alkanethiols on gold have been widely studied, and many of their properties have been reported throughout the literature.[36, 38, 39] Alkanethiol monolayers on gold are relatively easy to prepare for many reasons. The thiols generally dissolve well in ethanol, a common, non-hazardous solvent. The thiol/ethanol solution is not sensitive to water or other impurities so it can be used for long periods of times. The gold surface does not need to be treated prior to deposition because the thiols displace impurities adsorbed on the gold surface (such as adventitious carbon). Alkanethiols are also commercially available with many different terminal groups so that surfaces with different functionalities can be prepared and studied.

In our initial investigation, monolayers of varying thicknesses were deposited on gold via self-assembly of n-octadecanethiol ($C_{18}SH$), n-dodecanethiol ($C_{12}SH$), n-octanethiol (C_8SH), 11-mercapto-1-undecanol ($HO\text{-}C_{11}SH$), and 11-mercapto-1-

undecanoic acid ($HO_2CC_{10}SH$). To investigate the wetting properties of each monolayer, the advancing and receding contact angles of water, hexadecane, and [$bmim^+$][$triflate^-$] (IL) were measured and are shown in Table 1.

Table 1. Wetting Properties of SAMs on Au

Adsorbate	θ_{H2O}[a] (°) (adv, rec)	θ_{HD}[b] (°) (adv, rec)	θ_{IL}[a] (°) (adv, rec)
$C_{18}SH$	112, 102	49, 40	69, 64
$C_{12}SH$	109, 96	46, 30	64, 60
C_8SH	106, 98	43, 32	66, 58
$HOC_{11}SH$	28, 19	<15, --	17, --
$HO_2CC_{11}SH$	38	n/a	n/a

Standard deviation = a.) ± 5; b.) ± 1.

Water and hexadecane contact angles are lower for monolayers formed from shorter alkanethiols. A homogeneous methyl surface typically gives water contact angles of 109-114°,[34] and hexadecane contact angles of ~47°.[40] Lower contact angles result when methylene groups are exposed on the surface because these groups are less hydrophobic and more oleophilic than the terminal methyl groups. Thus, the lower contact angles for shorter chained n-alkanethiols are consistent with the presence of more defects which allow the chains to expose their methylene groups. IL contact angles do not exhibit an apparent trend associated with adsorbate chain length. Since the surface tension of the IL falls between that of water (73 mN/m)[41] and hexadecane (27 mN/m),[41] the IL contact angle is between that of the water and hexadecane contact angle.

The hydroxyl-terminated SAM exhibits a low water contact angle because of the hydrophilic nature of the hydroxyl terminus. However, samples that were not

characterized immediately after removal from the $HOC_{11}SH$ solution had higher water contact angles (50-70°) because the high energy surfaces minimize themselves by adsorbing adventitious materials from the air. The value reported here was averaged only from samples that were characterized within 5 min after removal from solution. Still, the water contact angles are higher than some literature values,[36] which is probably a result of defects in the monolayer that expose methylene groups to the surface.

Alkyl Silane Monolayers

Modification of a silicon oxide surface with a monolayer is slightly more involved than that of gold surfaces. Silicon oxide surfaces must be treated with piranha solution to remove adventitious carbon and hydroxylate the SiO_2 into silanols that react with trichlorosilane head groups. Solutions of trichlorosilanes must be prepared in anhydrous solvents and in dry conditions since they react rapidly with hydroxyl groups. The presence of water leads to polymerization of precursor molecules, which will hinder and/or prevent the formation of close-packed monolayers, as schematically depicted previously in Figure 6. In this study, alkyl trichlorosilanes of varying lengths, including octadecyltrichlorosilane ($C_{18}SiCl_3$), hexadecyltrichlorosilane ($C_{16}SiCl_3$), dodecyltrichlorosilane ($C_{12}SiCl_3$), and octyltrichlorosilane (C_8SiCl_3) were used to form monolayers on piranha-treated silicon surfaces. An exposure time of ~5 h in solution yielded the most oleophobic surface without yielding thicknesses that suggested the presence of vertical polymerization.

Table 2. Characteristics of Hydrophobic SAMs on Si

Thickness of monolayer, d; contact angle, θ;

Adsorbate	d (Å)	θ_{H2O}[a] (°) (adv, rec)	θ_{HD}[b] (°) (adv, rec)	θ_{IL}[a] (°) (adv, rec)
$C_{18}SiCl_3$	24	110, 103	44, 40	70,65
$C_{16}SiCl_3$	19	110, 104	43, 42	---
$C_{12}SiCl_3$	14	110, 103	37, 32	69, 59
C_8SiCl_3	11	110, 100	32, 26	69, 56

Standard deviation = a) ± 5; b) ± 1.

While the advancing water contact angles are similar for all monolayers, the advancing hexadecane contact angles decrease with decreasing adsorbate chain length. Because methylene groups are oleophilic, hexadecane contact angles are more sensitive to the presence of methylene groups than are water contact angles. The decreasing hexadecane contact angles indicate that the monolayers formed from $C_{18}H_{37}SiCl_3$ and $C_{16}H_{33}SiCl_3$ exhibit a more homogeneous methyl surface than the monolayers formed from adsorbates with fewer carbons. The similar contact angles of the IL on these surfaces suggest that it is not sensitive to the presence of the methylene groups.

Figure 8 shows the effect of alkylsilane chain length on film thickness and indicates a general increase in film thickness as chain length is increased. The slope of a best fit line through these data indicate that each carbon contributes 1.3 Å to the thickness of the film.

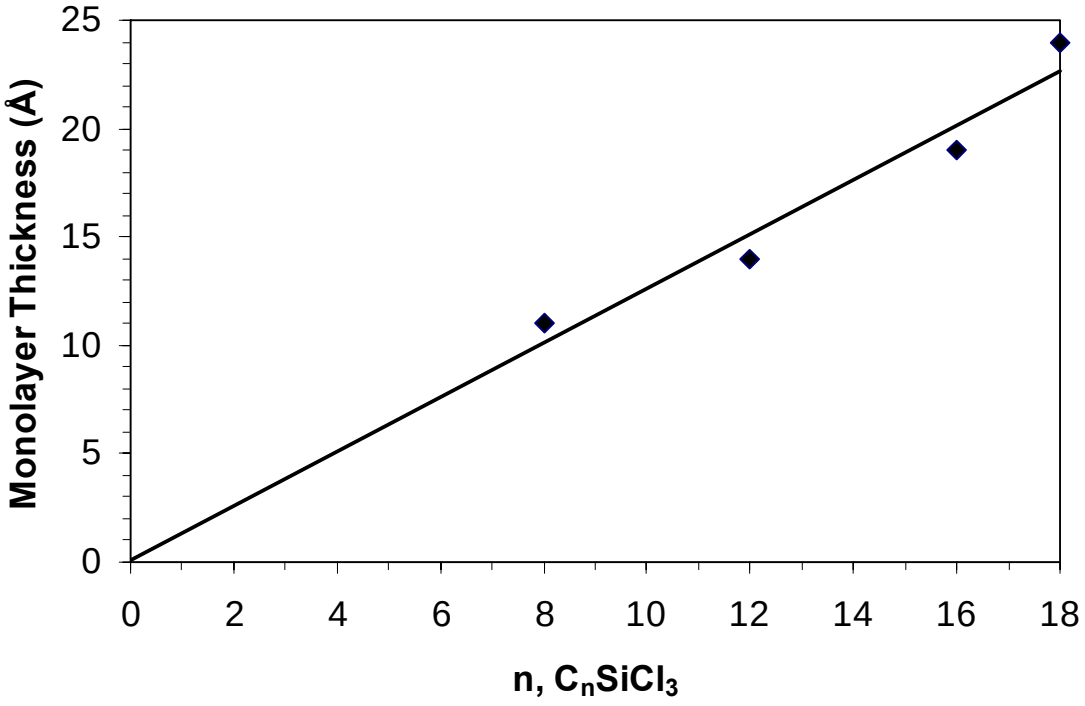

***Figure 8**. The thickness of the monolayer is plotted against number of carbons in the adsorbate. The slope of the fitted line is 1.3 Å/Carbon.*

Functionalized Silane Monolayers

Silane monolayers with different terminal groups were also studied. Fluorocarbon monolayers have lower surface energy than methyl-terminated monolayers and have been suggested for stiction reduction in MEMS.[16] Vinyl-terminated monolayers are hydrophobic, but they are oleophilic since most oils wet methylene-terminated surfaces. They can also be converted to hydroxyl-terminated monolayers, which will be important in future experiments. Piranha-treated silicon substrates were exposed to 1 mM solutions each of (tridecafluoro-1,1,2,2-tetrahydrooctyl)-1-trichlorosilane ($F_3C(CF_2)_5(CH_2)_2SiCl_3$) and 5-hexenyltrichlorosilane ($H_2C{=}C_5H_{10}SiCl_3$) in anhydrous toluene.

Thicknesses and contact angles reported in Table 3 indicate that fluorinated monolayers and vinyl-terminated monolayers were formed from $F_3C(CF_2)_5(CH_2)_2SiCl_3$ and $H_2C=C_5H_{10}SiCl_3$, respectively. (Monochlorosilanes were also briefly investigated, but their long deposition times and poor surface coverage rendered them less feasible for this work.)

Table 3. Characteristics of Functionalized SAMs on Si

Chemical Name	d (A)[a]	θ_{H2O}[b] (°) (adv, rec)	θ_{HD}[c] (°) (adv, rec)	θ_{IL}[d] (°) (adv, rec)
$F_3C(CF_2)_5(CH_2)_2SiCl_3$	10	125, 75	80, 55	83, 60
$H_2C=C_5H_9SiCl_3$	7	96, 84	<15	50, 33

Standard deviation = a.) ± 2; b.) ± 12; c.) ± 7; d.) ± 5

The advancing water contact angle indicates that the monolayer formed from $F_3C(CF_2)_5(CH_2)_2SiCl_3$ is very hydrophobic, yielding the highest advancing water contact angle of the adsorbates studied here. The water contact angle hysteresis, (θ_{adv}-θ_{rec}), is large, at ~50°, indicating a rough surface.[20] These fluorocarbon monolayers may exhibit high roughness due to impurities in the precursor solution, as discoloration in the chemical was observed. A fluorocarbon monolayer may inherently exhibit greater roughness than its hydrocarbon counterpart because fluorocarbon chains have a helical conformation and a large van der Waals radius that prevent them from packing as tightly as hydrocarbon chains.

For surfaces exposed to a precursor solution of $H_2C=C_5H_9SiCl_3$, the average advancing water contact angle was 96° which is consistent with literature values.[42] The

large deviation in water contact angles (ranging from 90° to 108°) was not correlated to precursor solution exposure time so monolayer formation from $H_2C=C_5H_9SiCl_3$ adsorbates is likely very sensitive to solution and ambient conditions. Though the vinyl-terminated monolayer is hydrophobic ($\theta_{H2O} > 90°$), it is oleophilic because is it wet by hexadecane. The IL is more compatible with a vinyl-terminated monolayer than with a methyl-terminated monolayer as indicated by the ~20° decrease in IL contact angle.

Step 2: Ionic Liquid Coating

After demonstrating that a variety of repeatable monolayers could be obtained, the coating properties of these monolayer surfaces were investigated. The ionic liquid, [bmim$^+$][triflate$^-$] (IL), was applied to a monolayer-coated substrate in a two-step process. In the first step, the IL was dissolved in a solvent at a concentration of 0.5% (w/v), and a 10 μL drop of this solution was applied to the substrate. In the second step, the substrate was immediately placed under vacuum to evaporate the solvent. In order to form an IL film on the surface, the drop solution must spread across the surface, and upon evaporation, the IL should remain as a film spread across the surface, as depicted in Figure 9a. Thus, by equations 2 and 3, the surface tension of the drop solution (IL and solvent) must be low enough for spreading to occur, and the surface energy of the substrate must be high enough to prevent the IL from beading up upon solvent evaporation, as shown in Figure 9b.

Initially, dichloromethane (DCM) was selected as a solvent. Because the IL was synthesized from DCM, we knew that the two were compatible and that the IL was soluble in DCM. However, the IL/DCM solution would not wet the low energy surfaces;

thus the IL could not spread across the sample to form a film. Clearly, a solvent with lower surface tension than DCM (26.5 mN/m)[36] was required to promote spreading. A polar solvent is needed to shield the electrostatic interactions between the IL cation and anion and promote dissolution of the IL. Ethanol, a readily available polar solvent that is less hazardous than DCM and has a surface tension of 22.1 mN/m[41] solvates the IL. Therefore, subsequent deposition utilized a 0.5% (w/v) solution of the IL in ethanol.

On a low energy SAM, even when the solvent would spread across the surface, the ionic liquid would bead up into tiny droplets on the surface, upon evaporation of the solvent, as depicted in Figure 9b. An exception was noticed for vinyl-terminated films that had been sitting out for a few days before IL deposition. The water contact angle of these samples was observed to have changed from ~95° (immediately after removal from solution), to ~60° after exposure the laboratory ambient for a few days. This observation led to the hypothesis that the critical surface energy necessary to accept a coating of the IL corresponds to a water contact angle of ~60°. To hone in on this critical regime, monolayers of varying surface energy were prepared and coated with the IL.

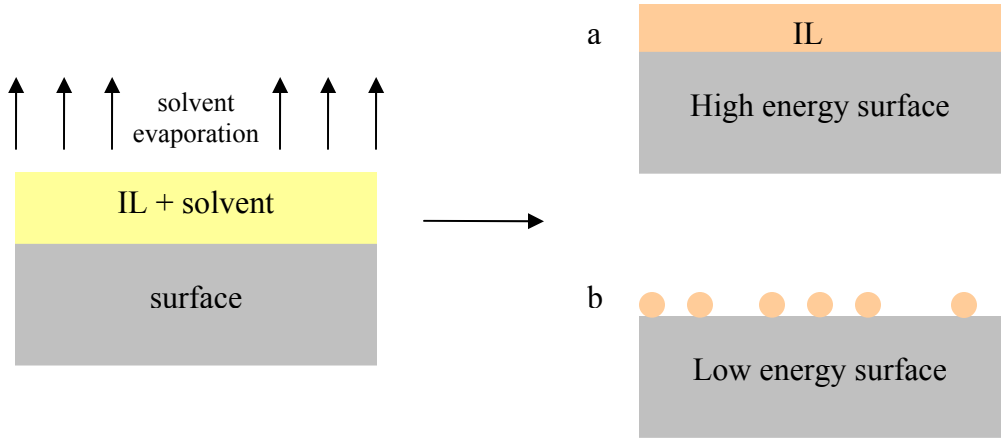

Figure 9. *Behavior of the IL upon drop casting. A solvent with low surface tension helped spread the IL across the surface. The solvent was then evaporated, leaving IL on the surface. On higher energy surfaces (a), the IL remained as a film spread across the surface, but on lower energy surfaces (b), the IL coalesced into droplets scattered across the surface.*

Mixed Monolayers on Gold

To determine the critical surface energy above which a film of the IL would coat a surface, mixed monolayers of varying surface concentrations of methyl and hydroxyl termini were prepared and coated with the IL by drop casting. For this study, thiol monolayers on Au were studied initially because mixed monolayers that exhibit a broad range of surface energies are straightforward to prepare on gold whereas high energy surfaces from silane monolayers require a more involved synthetic approach. In addition, IL films on gold can be characterized by RAIRS whereas IL films on silicon are not easily characterized by infrared spectroscopy.

Solution mixtures of $C_{12}SH$ and $HOC_{11}SH$ in ethanol were prepared such that each mixture had a total thiol concentration of 1 mM. By this method, surfaces with advancing water contact angles ranging from 28° to 110° were prepared. The advancing

water contact angle of each surface, (θ_{mixed}) was used to estimate the fractional surface coverage of methyl and hydroxyl termini within the monolayer from the equation proposed by Cassie[35]

$$\cos \theta_{mixed} = \sigma_1 \cos \theta_1 + (1-\sigma_1) \cos \theta_2 \quad (6)$$

where σ_1 is the fractional surface coverage of $C_{12}SH$, $(1-\sigma_1)$ is the fractional surface coverage of $HOC_{11}SH$, θ_1 is the water contact angle of a monolayer surface composed entirely of $C_{12}SH$, and θ_2 is the water contact angle of a monolayer surface composed entirely of $HOC_{11}SH$.

As shown in Figure 10, $C_{12}SH$ dominates the monolayer, even when the precursor solution was composed of only 10% $C_{12}SH$. The transition for hydroxyl-terminated molecules to dominate the monolayer occurred when the $C_{12}SH$ solution concentration was decreased from 10% to 5%, as the hydroxyl content in the SAM increased from 20% to 70%. Of the two precursor molecules, $HOC_{11}SH$ has a higher solubility in ethanol because of its polar terminus. Adsorption of the less soluble species is therefore favored, leading to the dominance of $C_{12}SH$ in the monolayer.[36]

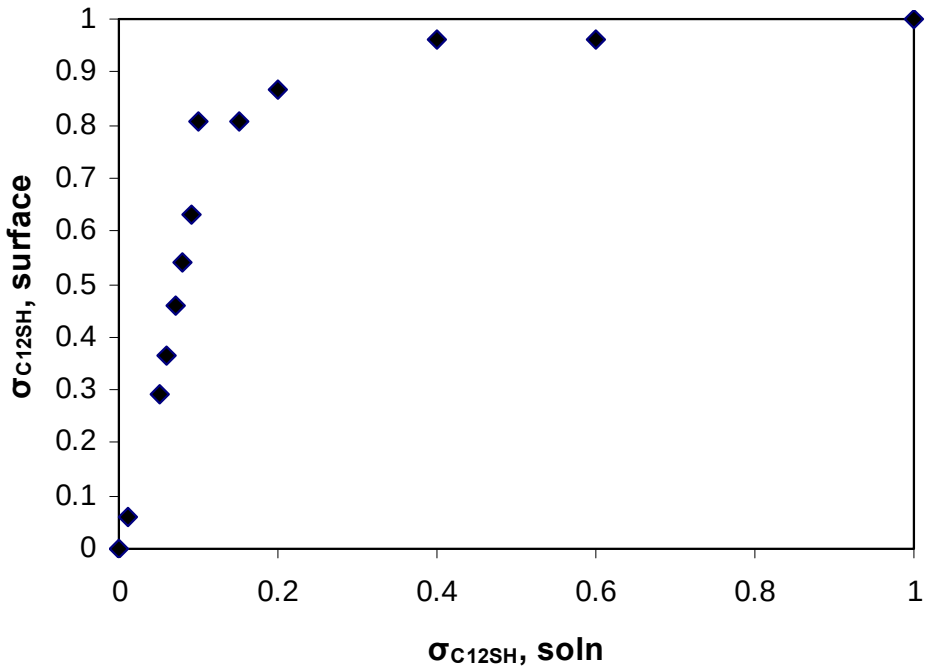

Figure 10. *Fraction of $C_{12}SH$ monolayer coverage resulting from 1mM total precursor solution mixture of $C_{12}SH$ and $HOC_{11}SH$ in ethanol. $C_{12}S$ dominates the monolayer even for very low $C_{12}SH$ solution concentrations.*

Drop Casting

IL films were drop cast from ethanol onto the mixed monolayers to determine if a smooth film would form. Figure 11 shows the IL films on monolayers with varying $C_{12}SH/HOC_{11}SH$ surface concentrations. The critical fractional $C_{12}SH$ coverage in a monolayer that could be coated by an IL thin film was 45% (± 2%) , which corresponds to a water contact angle of ~70°and an IL contact angle of 27°(+/-5°). Precursor solutions of less than 7% $C_{12}SH$ were required to achieve this monolayer coverage of sufficient hydroxyl coverage to enable IL film deposition.

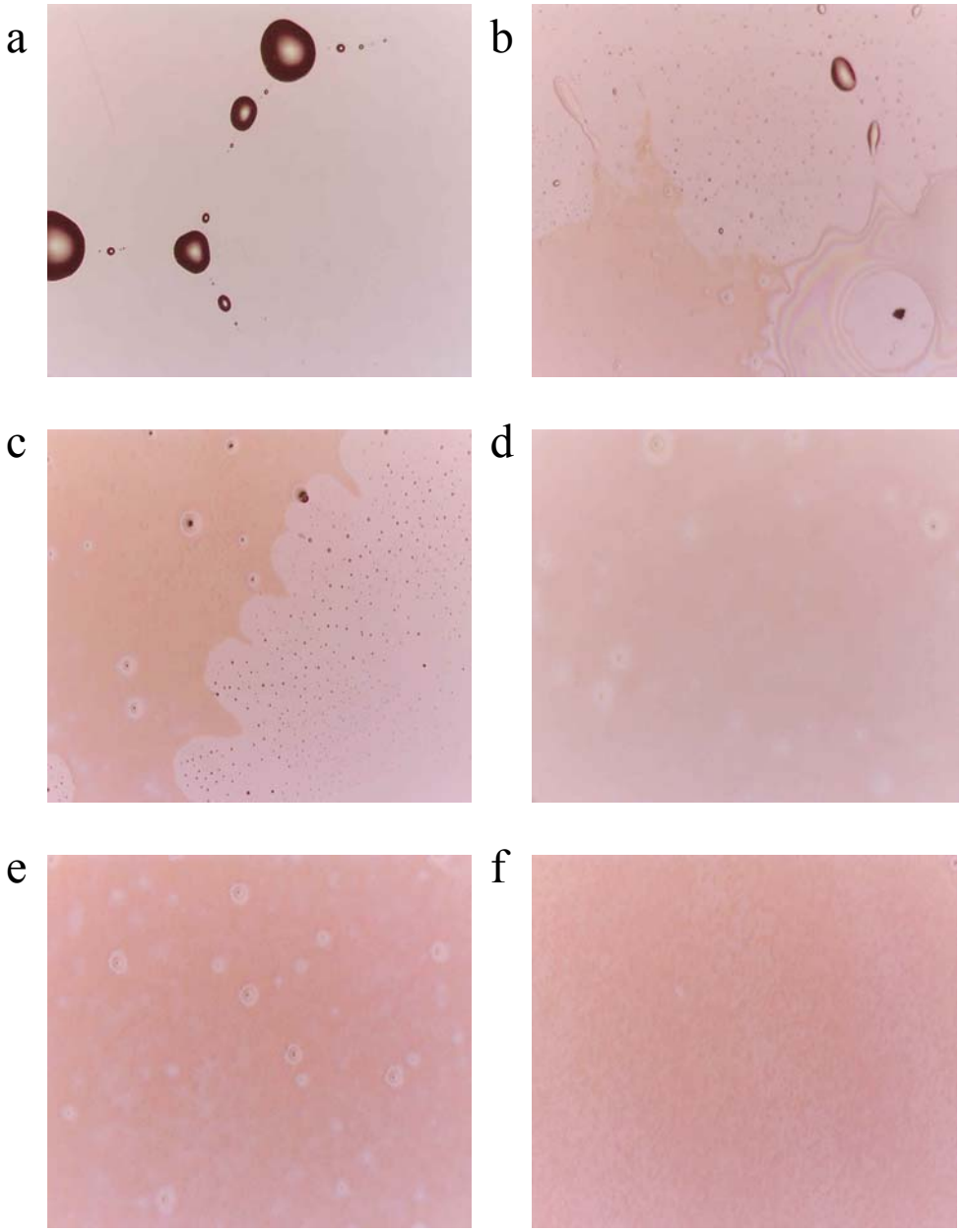

Figure 11. *Microscope images of IL films on mixed monolayers of CH_3- and OH-terminated alkanethiols on gold with CH_3 surface concentration, water contact angle of a.) 81%, 95°, b.) 54%, 76.5°, c.) 47%, 71°, d) 43%, 70°, e.) 39%, 68°, f.) 36%, 63.5°. Data are from multiple experiments. All samples exhibited multiple regions, but the images shown here depict the most prevalent region in the specified film.*

Spreading of the IL drop solution (IL + solvent) did not occur on surfaces with a fractional $C_{12}SH$ coverage of greater than 47%. However, two different wetting regimes were observed in this region. Though spontaneous spreading did not occur on surfaces with a fractional $C_{12}SH$ coverage between 47% and 87%, when samples were tilted, the drop moved across the surface leaving a thin film behind, suggesting that the receding contact angle of the IL drop solution (IL + solvent) on the surface was ~0. However, due to the high surface tension of the IL as compared to the IL drop solution (IL + solvent), after the solvent was evaporated, the ionic liquid coalesced into tiny droplets scattered across the surface, rather than spreading out into a film. In the second regime, samples with a fractional $C_{12}SH$ coverage of greater than 87% were never wet by the IL/ethanol drop, even as the drop was rolled around on the surface. Under vacuum, the IL/ethanol drop shrunk into a smaller drop of IL as the ethanol evaporated. Thus, the surface energies characteristic of these two regimes are too low to be compatible with an IL film, though the former regime is characterized by a surface energy high enough to be compatible with a film of the IL/ethanol solution.

Mixed Monolayers on Si

A variation in surface energy on silicon substrates was produced by partially oxidizing a vinyl-terminated trichlorosilane monolayer. Piranha-treated silicon samples were submerged in a 1 mM solution of varying ratios of methyl- and vinyl-terminated 8-carbon alkyltrichlorosilanes in anhydrous toluene for 1-3 h. A few piranha-treated samples were submerged in a 1 mM solution of 5-hexenyltrichlorosilane in anhydrous toluene for 1-3 h, for comparison. Immediately upon removal from solution, samples

were characterized or oxidized in the following manner. Under nitrogen atmosphere, the samples were treated with a borane·THF complex for 10-20 min and rinsed with anhydrous THF. Samples were then removed from the nitrogen atmosphere, rinsed with copious amounts of water, and submerged in a heated (1:1:5) solution of ammonium hydroxide, H_2O_2, and water for 15-60 min. Immediately upon removal from the hydroxide solution, samples were rinsed with copious amounts of water, dried, and characterized by contact angle analysis or coated by drop casting.

Upon drop casting, the IL beaded up on the samples with water contact angles greater than 76°, as shown in Figure 12. The sample with the 74° water contact angle (Figure 12 c) showed a transition state in film formation. The IL neither beaded up nor formed a continuous film. To the naked eye, the surface appeared to have a continuous film, but microscope images showed that it consisted of tiny, closely-spaced but disconnected islands of IL. Because the IL formed closely-spaced islands rather than droplets, this surface must be close to the critical surface energy at which a continuous film begins to form. Indeed, a more continuous film was formed on the surface with a 67° water contact angle (Figure 12 b), and a continuous film was formed on the surface with a 56° water contact angle (20°, +/-5° IL contact angle). Similar to the results from IL deposition on a SAM-coated gold substrate, surfaces below a critical water contact angle of 70° (+/-4°) support a sufficient IL coating by drop casting from ethanol.

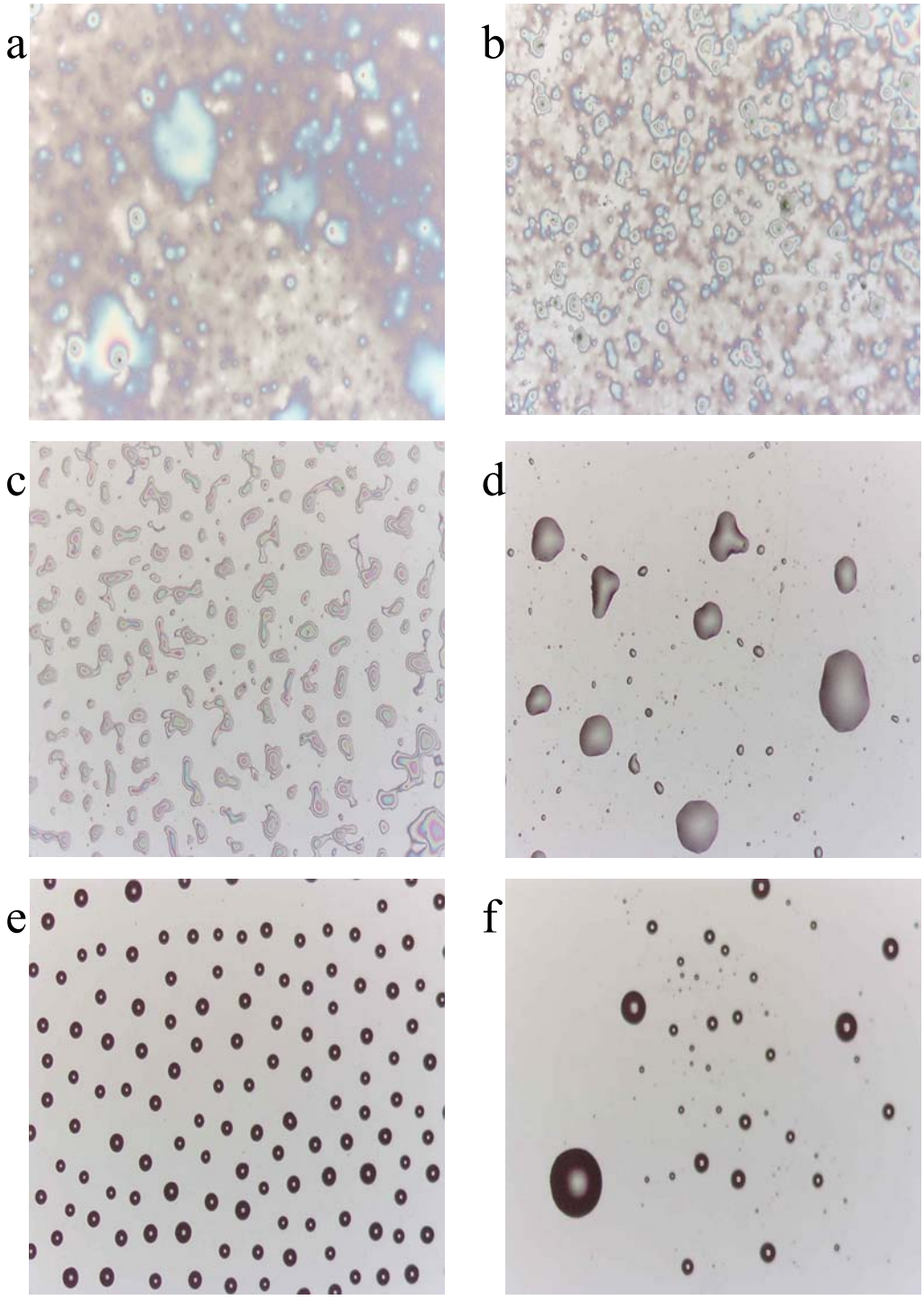

***Figure 12**. Microscope images from IL drop cast onto modified Si surfaces with water contact angles of a.) 56°, b.) 67°, c.) 74°, d.) 76°, e.) 87°, f.) 101°. Images are taken under a microscope magnified 5x. The films with water contact angles below 77° all contained regions of both a very continuous film and a very sparsely distributed film. The images shown here depict the most prevalent region in the specified film.*

FTIR Analysis of IL Film

FTIR spectra of the [$bmim^+$][$triflate^-$] (IL) films were obtained to provide information on film composition and structure. The effects of film thickness, casting solvent, and underlying surface were investigated. A transmission IR spectrum of the bulk IL was obtained after placing a thick drop of IL on a NaCl crystal. Thin and thick films of IL were deposited onto carboxylic acid- and hydroxyl-terminated surfaces, and RAIRS was used to characterize the IL films. A 'thin film' (~50 nm) of IL was drop cast onto a surface from a dilute solution in ethanol or DCM, as described previously. A 'thick film' (~1 μm) of the IL was applied to a surface by placing a drop of the IL onto the surface and tilting the sample to spread the IL into a thick coating.

Figure 13 presents the FTIR spectra of the bulk IL, a thick film of IL, and a thin film of IL. In the high frequency region (3200-2800 cm^{-1}) of the IR spectra, the ionic liquid exhibits five major peaks due to hydrocarbon stretching in the butyl and methyl side chains. (Refer to Figure 7 for a schematic of the structure of the IL.) In region of 1600-1266 cm^{-1}, peaks arise from C-H, C-N and ring stretching vibrations in the cation.[43] The region of 1350-1030 cm^{-1} uniquely contains peak contributions from both the cation and the triflate anion, with the triflate anion contributing peaks due to asymmetric SO_3 stretching at 1305-1240 cm^{-1}, symmetric CF_3 stretching at 1224-1227 cm^{-1}, asymmetric CF_3 stretching at 1175 cm^{-1}, and symmetric SO_3 stretching at 1036-1032 cm^{-1}.

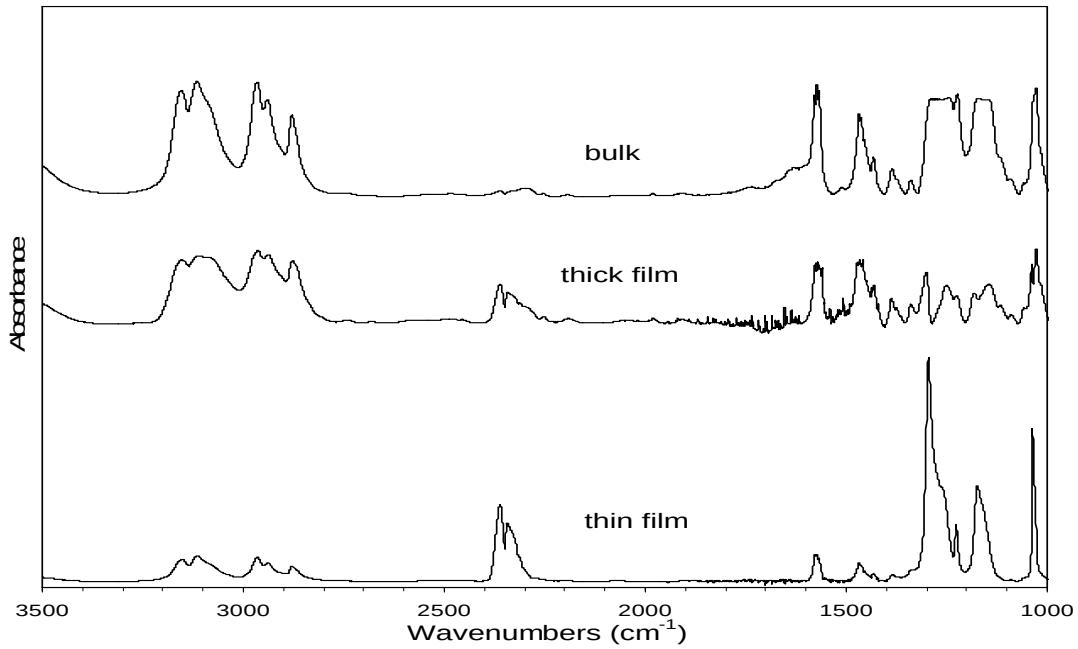

Figure 13*. Transmission FTIR spectrum of the bulk IL and RAIR spectra of a thick (~2 μm) and thin (~50 nm) IL film are compared. Peaks in the region of 2800-3300 cm^{-1} result from C-H stretching in the imidazolium ring, peaks in the region of 1600 – 1300 cm^{-1} result from C-N stretching in the imidazolium ring, and peaks in the region of 1300-1030 cm^{-1} result from stretching vibrations in the both the ring and in the triflate anion. The bulk spectrum represents isotropic orientation of the ions; thus the inflated peaks in the triflate region in the thin film suggest the anisotropy of the anion.*

Effects of Film Thickness

As shown in Figure 13, the bulk IL exhibits peaks in the low frequency region that are of the same general intensity as the peaks in the high frequency (C-H stretching) region. By the nature of the experiment, the transmission FTIR spectrum of the bulk IL yields peaks which are characteristic of isotropic orientation of the IL molecules. Thus, because peaks in the thick film exhibit this same trend of similar peak intensity across the spectrum, molecules in the thick film also exhibit isotropic orientation. The thin film uniquely exhibits peaks at ~1293 cm^{-1}, ~1226 cm^{-1}, 1175 cm^{-1}, and 1035 cm^{-1} that are the

same intensity or significantly more intense (by nearly an order of magnitude) than those in the C-H stretching region, suggesting a deviation from isotropy occurs in the thin film. Further evidence of anisotropy in the thin film is found when comparing the absolute intensities of peaks in the thick and thin films.

As shown in Figure 14, the five major peaks in the C-H stretching region (2800-3200 cm^{-1}) of the thick and thin films have similar peak placement and are consistent with peak placement in the bulk IL spectrum. However, the intensity of the peaks in the thick film is ~5 times greater than in the thin film in this region. This trend of greater peak intensity in the thick film is observed in the 1600-1320 cm^{-1} region as well.

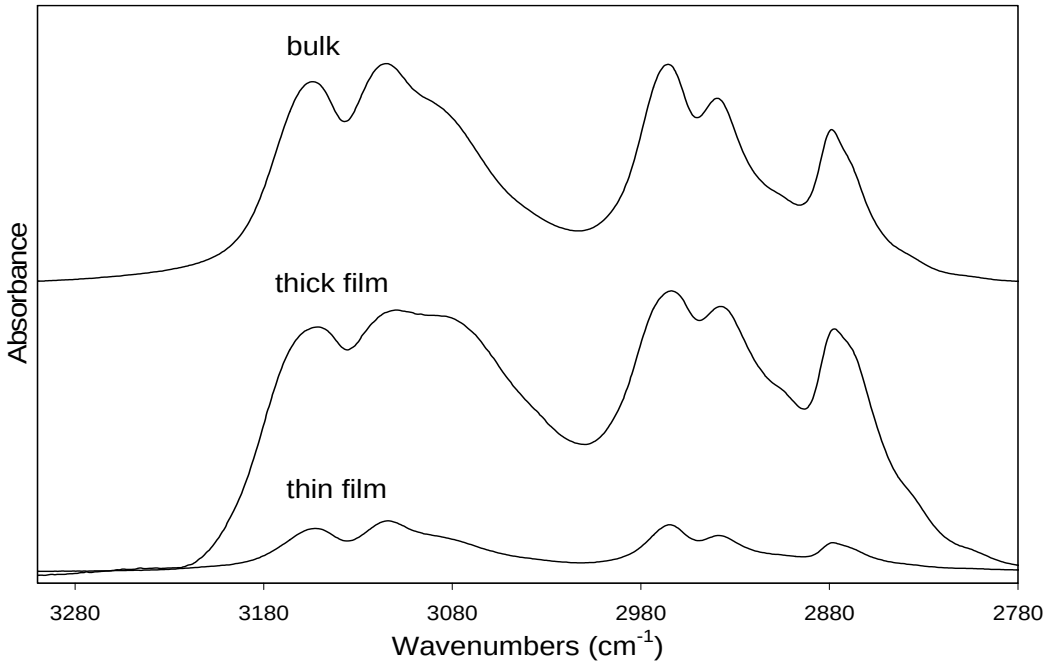

Figure 14*. Transmission FTIR spectrum of the C-H stretching region for the IL in bulk, and RAIR spectra of a thick and a thin film of the IL. All peaks in the bulk are represented in spectra of the two films. Peaks exhibit much larger intensity in the thick film. The bulk spectrum has been offset for clarity, while spectra from the thin and thick films overlap to compare peak intensity.*

In general, peaks of greater intensity are expected in the thicker film because of the presence of a greater number of molecules. However, as shown in Figures 13 and 15, the intensity of the peaks at ~1293 cm^{-1}, ~1226 cm^{-1}, 1175 cm^{-1}, and 1035 cm^{-1} in the thin films increased or remained at a comparable magnitude to those in the thick film, rather than decreasing in intensity. As stated previously, the spectra for the thick and thin films were obtained using RAIRS, which is sensitive to molecular orientation because only transition dipole moments with a component normal to the surface generate peaks. Thus, if molecules in the thick film are randomly oriented as deduced above, molecules in the thin film must be consistently oriented with certain transition dipole moments generally normal to the surface in order to yield a RAIR spectrum with peaks of equal or greater intensity than those generated from the thick film. These large peaks observed in the spectrum for the thin film are consistent with previously reported[44-46] peak assignments for the triflate anion. Specifically, the peak at ~1293 cm^{-1} is due to asymmetric SO_3 stretching (1305-1240 cm^{-1}), the peak at ~1226 cm^{-1} is due to symmetric CF_3 stretching (1224-1227 cm^{-1}), the peak at ~1175 cm^{-1} corresponds to asymmetric CF_3, and the peak at 1035 cm^{-1} is due to symmetric SO_3 stretching (1036-1032 cm^{-1}). As shown in Figure 15, the peaks that are associated with asymmetric bond vibrations in the anion are larger than the symmetric vibrations, suggesting that the anion is oriented with asymmetric transition dipole moments generally more along the surface normal than the symmetric moments.

Also shown in Figure 15, about half the peaks that are observed in the spectrum for the thick film do not appear in the spectrum for the thin film in the 1305-1035 cm^{-1} range. This observation suggests that the cation orients itself in the thin film so that

certain ring stretching vibrations align parallel to the substrate and do not generate peaks. Thus, results suggest that the triflate anion orients itself in the thin film such that its asymmetric SO_3 and CF_3 stretching vibrations are more normal to the surface, while the cation orients itself in such a way that certain ring stretching vibrations are parallel to the surface. Further information about cation orientation may be extrapolated from Fitchett and Conboy[47] who investigated the orientation of the cation of similar ionic liquids at a SiO_2 surface. They proposed that the imidazolium ring was oriented between 16° and 32° from the surface normal with the side chains oriented ~37° from the surface normal.[47] The results presented here do not refute that possibility; thus, the cations of the IL in this study may exhibit a similar orientation.

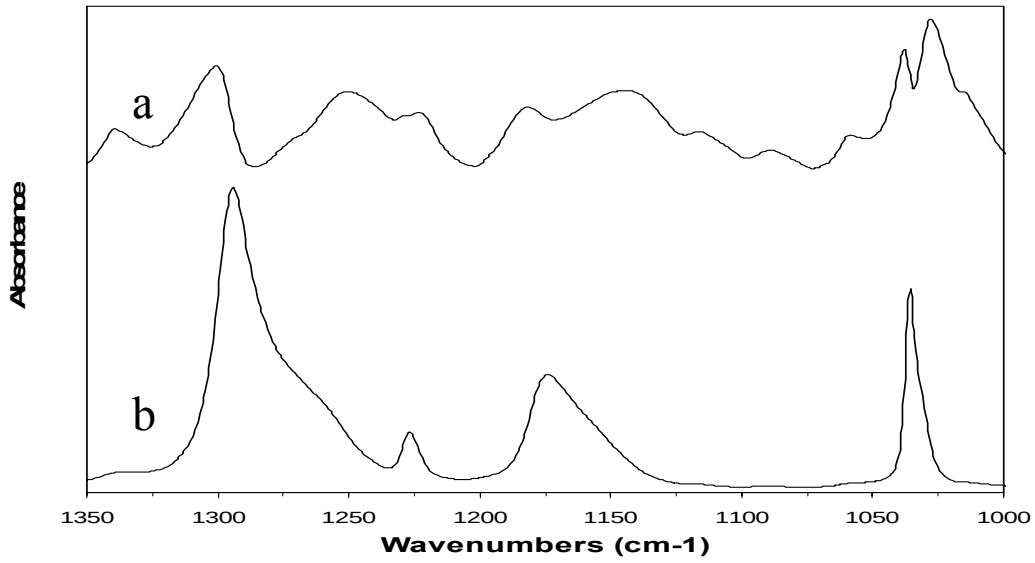

Figure 15*. The triflate region of a RAIR spectrum for a) thick film of the IL and b) thin film of the IL, on a monolayer surface. Peaks are assigned as SO_3 asymmetric stretching at 1300-1250 cm^{-1}, CF_3 symmetric stretching at 1227 cm^{-1}, CF_3 asymmetric stretching at 1173 cm^{-1}, and SO_3 symmetric stretching at 1033-1037 cm^{-1}. The thick film spectrum has been offset for clarity.*

Effect of underlying surface and solvent

Neither the underlying surface of a thin film nor the solvent used to cast the thin film correlate strongly with features in the FTIR spectra as demonstrated in Figures 16 and 17. FTIR analysis showed that the solvent evaporated completely from the thin films. An OH-stretching band would be present in the region of 3200-3550 cm^{-1} if ethanol had not fully evaporated from the film.[43] If DCM had not fully evaporated from the film, the spectra of films cast from DCM would differ from those cast from ethanol in the 2900-3100 cm^{-1} due to C-H stretching, in the 1300-1150 cm^{-1} region due to CH_2-Cl wagging, and around 700-800 cm^{-1} from the C-Cl stretching vibration.[43] Thin films cast from DCM and ethanol exhibit similar peaks in this region (Figure 16) indicating no presence of solvent.

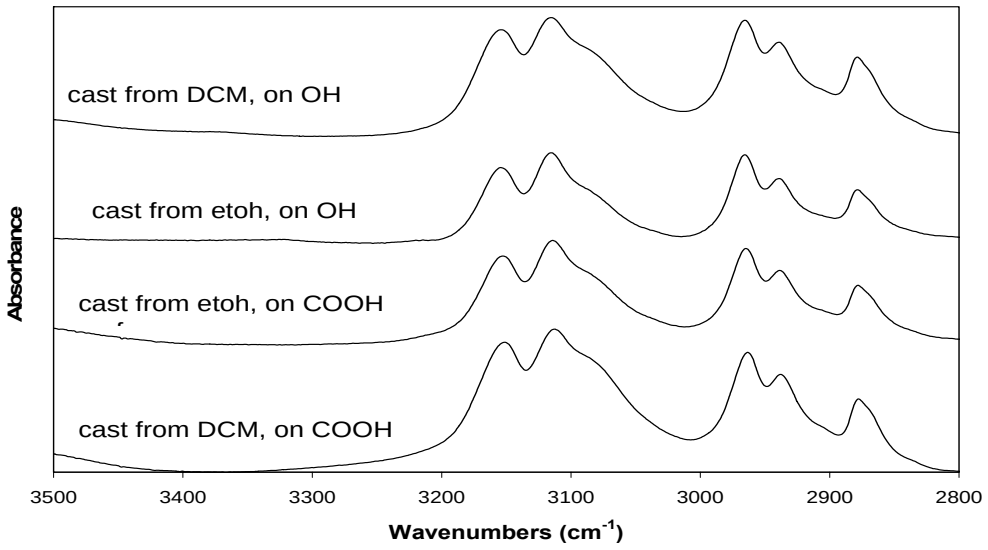

Figure 16*. The C-H stretching region of RAIR spectra from thin IL films cast from ethanol or DCM on functionalized SAMs on Au. Neither casting solvent nor surface functionality appear to have an impact on the FTIR spectra of the thin films. Spectra are offset for clarity.*

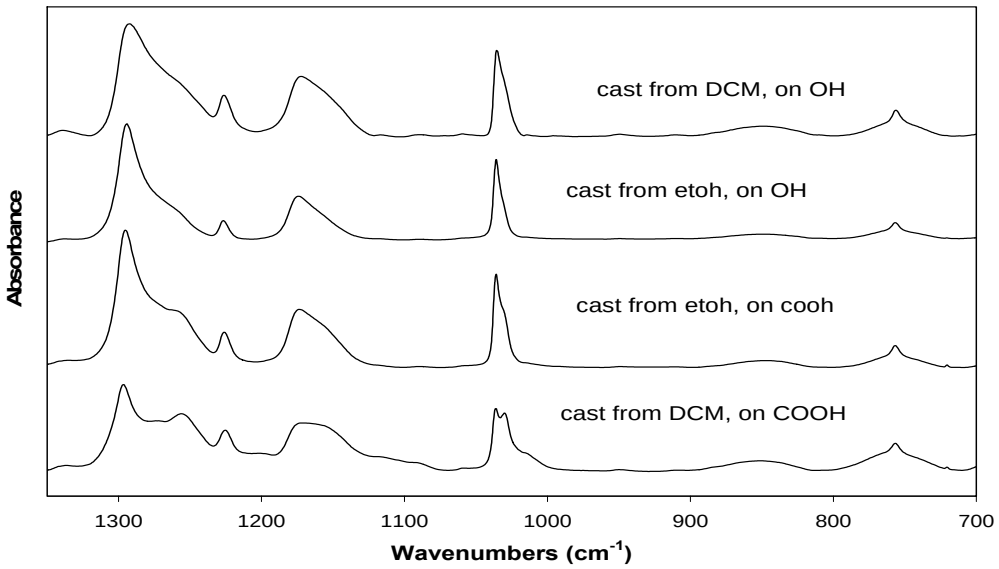

Figure 17*. The low frequency region of RAIR spectra from thin IL films cast from ethanol or DCM on functionalized SAMs on Au. Variation in the solvent used to cast the film and variation in the functional group of the surface under the IL thin film does not have a direct correlation to FTIR peaks in the thin film. Spectra are offset for clarity.*

CHAPTER V

CONCLUSIONS AND FUTURE WORK

In this work, Au and Si substrates were modified by depositing monolayers. The ionic liquid bmim triflate (IL) was synthesized to be applied as a mobile film on top of the monolayer-covered surfaces.

Initially, low-energy hydrophobic monolayers on Au and Si substrates were prepared from n-alkanethiols and from a variety of alkyltrichlorosilanes, respectively. The thicknesses of these monolayers increased as the chain length of the adsorbate molecules increased. Specifically, for n-alkyltrichlorosilanes, each carbon in the adsorbate chain contributed ~1.3 Å to the thickness of the monolayer film.

The IL would not coat these low-energy monolayer surfaces, thus monolayers of varying surface energy were prepared on both Au and Si surfaces to determine the critical surface energy above which the IL would coat a surface. On both Au and Si substrates, the critical surface energy required for the formation of an IL film was characterized by an IL contact angle of ~27° (± 5°), which corresponds to an advancing water contact angle of 70° (± 4°). Transmission FTIR studies of the bulk IL and RAIRS studies of IL films indicate that molecular orientation occurs in thin films (~50 nm) of IL but not in thicker films (~1 μm). Specifically, the triflate anion orients itself in the thin film such that its transition dipoles due to asymmetric SO_3 and CF_3 stretching are more normal to the surface, while the cation orients itself such that its transition dipoles due to ring

stretching characterized by vibrations at 1300-1000 cm^{-1} are oriented parallel with the surface.

This work has provided a foundation for future investigations of ionic liquid coatings on monolayers. Further work will include investigations using various ionic liquids that have lower surface tensions and viscosities. The behavior of the ionic liquid thin film at a solid interface will be investigated further using RAIRS and electrochemical impedance spectroscopy (EIS). Finally, monolayer films, ionic liquid films, and monolayer-ionic liquid dual-films will be investigated using nanotribological methods to assess their potential as replenishable lubrication schemes for MEMS devices.

REFERENCES

1. Romig, A. D.; Dugger, M. T.; McWhorter, P. J., Materials issues in microelectromechanical devices: science, engineering, manufacturability and reliability. *Acta Materialia* **2003,** 51, (19), 5837-5866.

2. Satyanarayana, N.; Sinha, S., Tribology of PFPE overcoated self-assembled monolayers deposited on Si surface. *Journal of Physics D: Applied Physics* **2005,** 38, 3512-3522.

3. Yu, B.; Zhou, F.; Mu, Z.; Liang, Y.; Liu, W., Tribological properties of ultra-thin ionic liquid films on single-crystal silicon wafers with functionalized surfaces. *Tribology International* **2006,** 39, 879-887.

4. Irving, D. L.; Brenner, D. W., Diffusion on a Self-Assembled Monolayer: Molecular Modeling of a Bound + Mobile Lubricant. *Journal of Physical Chemistry B* **2006,** 110, 15426-15431.

5. Choi, J.; Morishita, H.; Kato, T., Frictional Properties of bilayered mixed lubricant films on an amorphous carbon surface: effect of alkyl chain length and SAM/PFPE portion. *Applied Surface Science* **2004**, (228), 191-200.

6. Eapen, K.; Patton, S.; Zabinski, J., Lubrication of microelectromechanical systems using bound and mobile phases of Fomblin Zdol. *Tribology Letters* **2002,** 12, (1), 35.

7. Eapen, K.; Patton, S.; Smallwood, S.; Phillips, B.; Zabinski, J., MEMS Lubricants Based on Bound and Mobile Phases of Hydrocarbon Compounds: Film Deposition and Performance Evaluation. *Journal of Microelectromechanical Systems* **2005,** 14, (5), 954-960.

8. Satyanarayana, N.; Sinha, S. K.; Ong, B. H., Tribology of a novel UHMWPE/PFPE dual-film coated onto Si surface. *Sensors and Actuators A* **2006,** 128, 98-108.

9. Hoffmann, M.; Heitz, M.; Carr, J.; Tubbs, J., Surfactants in Green Solvent Systems: Current and Future Research Directions. *Journal of Dispersion Science and Technology* **2003,** 24, (2), 155-171.

10. Mu, Z.; Zhou, F.; Zhang, S.; Liang, Y.; Weimin, L., Effect of the functional groups in ionic liquid molecules on the friction and wear behavior of aluminum alloy in lubricated aluminum-on-steel contact. *Tribology International* **2005,** 38, 725-731.

11. Jimenez, A. E.; Bermudez, M. D.; Iglesias, P.; Carrion, F. J.; Martinez-Nicolas, G., 1-N-alkyl -3-methylimidazolium ionic liquids as neat lubricants and lubricant additives in steel-aluminium contacts. *Wear* **2006,** 260, (7-8), 766-782.

12. Liu, W.; Ye, C.; Gong, Q.; Wang, H.; Wang, P., Tribological Performance of Room-Temperature Ionic Liquids as Lubricant. *Tribology Letters* **2002,** V13, (2), 81-85.

13. Wang, H.; Lu, Q.; Ye, C.; Liu, W.; Cui, Z., Friction and wear behaviors of ionic liquid of alkylimidazolium hexafluorophosphates as lubricants for steel/steel contact. *Wear* **2004,** 256, 44-48.

14. Ye, C.; Liu, W.; Chen, Y.; Yu, L., Room-temperature ionic liquids: a novel versatile lubricant. *Chemical Communications* **2001**, 2244-2245.

15. Israelachvili, J., *Intermolecular and Surface Forces*. 2nd ed.; Academic Press Inc: San Diego, CA, 1992; p 450.

16. Srinivasan, U.; Houston, M. R.; Howe, R. T.; Maboudian, R., Alkyltrichlorosilane-Based Self-Assembled Monolayer Films for Stiction Reduction in Silicon Micromachines. *Journal of Microelectromechanical Systems* **1998,** 7, (2), 252-260.

17. Bhushan, B.; Israelachvili, J. N.; Landman, U., Nanotribology: friction, wear and lubrication at the atomic scale. *Nature* **1995,** 374, 607-616.

18. Khatri, O. P.; Biswas, S. K., Boundary lubrication capabilities of alkylsilane monolayer self-assembled on aluminum as investigated using FTIR spectroscopy and nanotribometry. *Surface Science* **2006,** 600, 4399-4404.

19. Sambasivan, S.; Hsieh, S.; Fischer, D. A.; Hsu, S. M., Effect of self-assembled monolayer film order on nanofriction. *Journal of Vacuum Science Technology A.* **2006**, (24), 1484.

20. Yoshizawa, H.; Chen, Y.-L.; Israelachvili, J., Fundamental Mechanisms of Interfacial Friction. 1. Relation between Adhesion and Friction. *Journal of Physical Chemistry* **1993**, (97), 4128-4140.

21. Liu, X.; Zhou, F.; Liang, Y.; Liu, W., Tribological performance of phosphonium based ionic liquids for an aluminum-on-steel system and opinions on lubrication mechanism. *Wear* **2006,** 261, (10), 1174-1179.

22. Li, J.; Shen, Y.; Zhang, Y.; Liu, Y., Room-temperature ionic liquids as media to enhance the electrochemical stability of self-assembled monolayers of alkanethiols on gold electrodes. *Chem Commun* **2005**, 360.

23. Wilkes, J. S.; Zaworotko, M. J., Air and water stable 1-ethyl-3-methylimidazolium based ionic liquids. *J Chem Soc - Chemical Comminications* **1992**, 965-967.

24. Phillips, B. S.; Mantz, R. A.; Trulove, P. C.; al, e., Surface Chemistry and tribological behavior of ionic liquid boundary lubrications additives in water. *American Chemical Society: Washington 2005* **2005,** 901, 244-253.

25. Yu, G. Q.; Zhou, F.; Liu, W. M.; al, e., Preparation of functional ionic liquids and tribological investigation of their ultra-thin films. *Wear* **2006,** 260, (9-10), 1076-1080.

26. Wibbeler, J.; Pfeifer, G.; Hietschold, M., Parasitic charging of dielectric surfaces in capacitive microelectromechanical systems (MEMS). *Sensors and Actuators A: Physical* **1998,** 71, (1-2), 74-80.

27. Bonhote, P.; Dias, A.; Popageoriou, N.; Kalyanasundaram, K.; Gratzel, M., Hydrophobic, highly conductive ambient-temperature molten salts. *Inorganic Chemistry* **1996,** 35, 1168-78.

28. Chen, M.-S.; Brandow, S. L.; Schull, T. L.; Chrisey, D. B.; Dressick, W. J., A Non-Covalent Approach for Depositing Spatially Selective Materials on Surfaces. *Advanced Functional Materials* **2005,** 15, 1364-1375.

29. Stevens, M., Thoughts on the Structure of Alkylsilane Monolayers. *Langmuir* **1999,** 15, 2773.

30. Britt, D. W.; Hlady, V., An AFM Study of the Effects of Silanization Temperature, Hydration, and Annealing on the Nucleation and Aggregation of Condensed OTS Domains on Mica. *JOURNAL OF COLLOID AND INTERFACE SCIENCE* **1996,** 178, 775.

31. Flinn, D. H.; Guzonas, D. A.; Yoon, R. H., Characterization of silica surfaces hydrophobized by octadecyltrichlorosilane. *Colloids and Surfaces A: Physicochemical and Engineering Aspects* **1994,** 87, 163.

32. McGovern; Kallury, M. E.; K.M.R; Thompson, M., Role of Solvent on the Silanization of Glass with Octadecyltrichlorosilane. *Langmuir* **1994,** 10, 3607.

33. Fadeev, A. Y.; McCarthy, T. J., Self-Assembly Is Not the Only Reaction Possible between Alkyltrichlorosilanes and Surfaces: Monomolecular and Oligomeric Covalently Attached Layers of Dichloro-and Trichloroalkylsilanes on Silicon. *Langmuir* **2000,** 16, 7268.

34. Wang, M.; Liechti, K. M.; Wang, Q.; White, J. M., Self-Assembled Silane Monolayers: Fabrication with Nanoscale Uniformity. *Langmuir* **2005,** 21, 1848-1857.

35. Cassie, A. B. D., Contact Angles. *Discussions of the Faraday Society* **1948,** 3, 11-16.

36. Bain, C. D.; Evall, J.; Whitesides, G. M., Formation of Monolayers by the Coadsorption of Thiols on Gold - Variation in the Head Group, Tail Group, and Solvent. *Journal of the American Chemical Society* **1989,** 111, (18), 7155-7164.

37. Patton, S. T.; Zabinski, J. S., Fundamental studies of Au contacts in MEMS RF switches. *Tribology Letters* **2005,** 18, (2), 215-230.

38. Bain, C. D.; Whitesides, G. M., Formation of Monolayers by the Coadsorption of Thiols on Gold - Variation in the Length of the Alkyl Chain. *Journal of the American Chemical Society* **1989,** 111, (18), 7164-7175.

39. Porter, M. D.; Bright, T. B.; Allara, D. L.; Chidsey, C. E. D., Spontaneously Organized Molecular Assemblies. 4. Structural Characterization of n-Alkyl Thiol Monolayers on Gold by Optical Ellipsometry, Infrared Spectroscopy, and Electrochemistry. *Journal of the American Chemical Society* **1987,** 109, 3559-3568.

40. Gupta, V. K.; Abbott, N. L., Azimuthal anchoring transition of nematic liquid crystals on self-assembled monolayers formed from odd and even alkanethiols. *Physical Review E* **1996,** 54, (5), R4540.

41. quest@surface-tension.de, Surface tension values of common test liquids for surface energy analysis. In www.surface-tension.de/: 2006.

42. Faucheux, N.; Schweiss, R.; Lutzow, K.; Werner, C.; Groth, T., Self-assembled monolayers with different terminating groups as model substrates for cell adhesion studies. *Biomaterials* **2004,** 25, (14), 2721-2730.

43. Silverstein, R. M.; Webster, F. X.; Kiemle, D. J., *Spectrometric Identification of Organic Compounds*. seventh ed.; John Wiley & Sons, Inc.: 2005.

44. Huang, W. W.; Frech, R.; Wheeler, R. A., Molecular-Structures and Normal Vibrations of Cf3so3- and Its Lithium Ion-Pairs and Aggregates. *Journal of Physical Chemistry* **1994,** 98, (1), 100-110.

45. Bernson, A.; Lindgren, J., Free ions and ion pairing/clustering in the system $LiCF_3SO_3$-PPO_n. *Solid State Ionics* **1993,** 60, 37-41.

46. Peterson, G.; Jacobson, P.; Torell, L. M., A Raman Study of Ion-Polymer and Ion-Ion Interactions in Low Molecular Weight Polyether-$LiCF_3SO_3$ Complexes. *Electrochemica Acta* **1992,** 37, (9), 1496-1497.

47. Fitchett, B. D.; Conboy, J. C., Structure of the Room-Temperature Ionic Liquid/SiO_2 Interface Studied by Sum-Frequency Vibrational Spectroscopy. *J. Phys. Chem. B* **2004,** 108, 20255-20262.